An Aurora Kinase A/TPX2 complex phosphorylates CKAP2 to control mitotic spindle growth

Thomas J Kucharski[1], Tatiana Lyalina[1] and Susanne Bechstedt[1,2*]

1) Department of Anatomy and Cell Biology, McGill University, Québec, Montréal, Canada, H3A 0C7

2) Centre de recherche en biologie structurale, McGill University, Québec, Montréal, Canada, H3G 0B1

*Lead Contact

Correspondence address:

Department of Anatomy and Cell Biology

3640 Rue University W-309

Montréal, Québec

Canada

H3A 0C7

Keywords: microtubule, mitosis, kinase, mitotic spindle, phosphorylation, Aurora, phosphatase

Summary

The formation of the mitotic spindle is a critical step in the equal separation of DNA from the mother cell to the two daughter cells. Cytoskeleton Associated Protein-2 (CKAP2) is a microtubule polymerase that associates with microtubules and centrosomes during interphase and mitosis. Loss of CKAP2 results in chromosomal instability and onset of aneuploidy. To identify proteins interacting with CKAP2, we immunoprecipitated endogenous CKAP2 together with interacting proteins from mitotic RPE1 cells and analysed the samples by mass spectrometry. This experiment identified the mitotic protein kinase Aurora Kinase A, together with its cofactor TPX2, as interacting proteins of CKAP2. Notably, CKAP2 co-localizes and interacts with Aurora Kinase A and TPX2 throughout mitosis, but not with the related protein Aurora Kinase B. Consistently, Aurora Kinase A phosphorylates CKAP2 both in mitotic cells and *in vitro*. Phosphorylated CKAP2 has reduced affinity for microtubules *in vitro*. Importantly, expression of Aurora A phospho-mimic mutants of CKAP2 in RPE1 cells results in phenotypes of a small mitotic spindle and reduced microtubule stability. Thus, Aurora Kinase A phosphorylates CKAP2 to regulate mitotic spindle growth and stability.

Introduction

The objective of mitosis is the equal partitioning of chromosomes into the two daughter cells. Upon initiation of mitosis, the nuclear envelope breaks down, and the mitotic spindle is formed. The mitotic spindle is comprised of bundles of microtubules (MTs), which are polymers of tubulin subunits[1]. During early mitosis, MTs attach to chromosomes at the kinetochore and pull them toward the metaphase plate. When all chromosomes are correctly attached to the spindle and aligned on the metaphase plate, such that both sister kinetochores are attached to MTs emanating from opposite spindle poles, the MTs then pull the sister chromatids apart into the two daughter cells[2,3]. Importantly, MTs are highly dynamic structures which can grow or shrink to generate pulling forces on chromosomes[1]. The growth and shrinkage rates of MTs must be tightly controlled to correctly align and segregate the chromosomes during mitosis[4–7]. The growth and shrinkage rates are controlled by a group of proteins known as Microtubule-Associated Proteins (MAPs)[1]. Amongst MAPs, the protein CKAP2 (alias TMAP) has generated substantial interest because it potently induces MT growth, its overexpression contributes to the onset of chromosomal instability and aberrant centrosome numbers, and its overexpression is associated with worse survival in cancer patients[8–14].

Studies on CKAP2 have revealed that the protein is phosphorylated on multiple sites during mitosis by both Aurora and Cyclin Dependent Kinases (CDKs). Phosphorylation of CKAP2 on conserved c-terminus sites by these kinases has been proposed to control the subcellular localization of CKAP2 during mitosis[8,15–19]. From early mitosis through anaphase, CKAP2 is localized on centrosomes and pole-proximal MTs. However, in late anaphase, CKAP2 abruptly changes localization and binds to chromosomes before it is finally degraded through the action of the Anaphase Promoting Complex/Cyclosome ubiquitin ligase during telophase/G1[8,15–

70 [20]. Thus, phosphorylation/dephosphorylation of CKAP2 has been proposed to function as a
71 switch to control the observed changes in protein localization. Phosphorylation sites in the n-
72 terminus of CKAP2 have also been detected in large-scale proteomics studies[21–23], but roles for
73 these phosphorylation sites have not yet been determined.

74 To gain insights into the molecular mechanisms that govern CKAP2 function, we
75 performed unbiased proteomic screening to identify CKAP2-interacting proteins. This approach
76 identified TPX2 and Aurora Kinase A (AurKA) as important interacting proteins of CKAP2. We
77 found that AurKA/TPX2 binds to and phosphorylates CKAP2 during mitosis to regulate its MT
78 binding and polymerase activity and thus control mitotic spindle growth and mitotic fidelity.
79 These new findings effectively integrate CKAP2 into existing spindle regulation pathways and
80 shed light on the regulation of this potent MT growth factor.

81 **Results**

82 **CKAP2 interacts with AurKA/TPX2 during mitosis**

83 To identify proteins that associate with CKAP2 during mitosis, we immunoprecipitated
84 endogenous CKAP2 together with interacting proteins from normal RPE-1 cells that were
85 synchronized in mitosis by sequential Palbociclib-STLC block (Figure 1A). 672 proteins were
86 identified by mass spectrometry in either or both CKAP2 immunoprecipitation or control
87 immunoprecipitation. To identify proteins that specifically associate with CKAP2, we applied
88 criteria of at least 4 identified peptides, and a 4:1 signal-to-noise ratio of peptides observed in the
89 CKAP2 vs control immunoprecipitations. This resulted in a high-confidence list of 90 unique
90 proteins that associate with CKAP2 in mitosis. To identify pathways in which CKAP2 might
91 participate, we performed gene ontology analysis on the set of 90 proteins. This analysis revealed
92 that CKAP2 participates in various cell division processes, as determined previously, as well as

93 RNA-related processes (Figure 1B). Search Tool for the Retrieval of Interacting Genes/Proteins
94 interaction network analysis revealed that CKAP2 associates with proteins that participate in
95 mitosis/chromatin organization (e.g. NCAPG), mRNA processing (e.g. CPSF1), and possibly
96 translation (e.g. RSL1D1) (Figure 1C). Amongst MAPs, we identified KIF2A, TXLNA,
97 KIF20A, TPX2, and KIF23 as CKAP2 potential interacting proteins. We also identified AurKA
98 as a CKAP2-interacting protein, which, although not a MAP as such, exists in cells mainly as a
99 heterodimer with TPX2, which is a MAP. We also identified numerous chromatin-bound proteins
100 that might mediate the interaction between CKAP2 and chromatin in late mitosis, including
101 TOP2A, SMC2, SMC4, NCAPG, NCAPD2, NCAPH, MACROH2A1 and KI67 (Figure 1C, 1D,
102 supplemental table 1).

103 Amongst CKAP2 interacting proteins that we detected, AurKA/TPX2 were of particular
104 interest. Aurora Kinase A phosphorylates numerous substrates at spindle poles and on MTs
105 during mitosis that broadly contribute to mitotic spindle growth, stability and function[24–27]. TPX2
106 binds directly to MTs and functions as an AurKA cofactor to localize AurKA to MTs and spindle
107 poles[28–30]. AurKA has been shown to be overexpressed in numerous cancers and contributes to
108 oncogenesis[31–33]. Critically, AurKA does not localize to MTs in the absence of TPX2[28].
109 Additionally, TPX2 has been demonstrated to directly contribute to MT growth, suggesting that
110 it may function in conjunction with CKAP2 in this capacity[29,30,34]. We first confirmed that
111 CKAP2 binds to the AurKA/TPX2 complex. We performed another CKAP2
112 immunoprecipitation from Palbociclib/STLC synchronized RPE-1 cells, but this time performed
113 Western blot analysis to probe for the presence of TPX2 and AurKA. This experiment confirmed
114 that both TPX2 and AurKA interact with CKAP2 (Figure 1E). We also performed the reciprocal
115 experiment, where we immunoprecipitated TPX2 and blotted for CKAP2 and Aurora A. This

116 experiment revealed a robust interaction with AurKA, as expected, and with CKAP2 (Figure
117 S1A).

118 AurKA is closely related to another mitotic kinase, Aurora Kinase B (AurKB). These two
119 kinases share a consensus motif R/K-R/K-x-S/T. Thus, both kinases are generally capable of
120 phosphorylating the same substrates. However, while TPX2 localizes AurKA to spindle poles
121 and MTs, INCENP localizes AurKB to centromeres and kinetochores[24–27,35–37]. Thus, AurKA and
122 AurKB are spatially separated in cells, which governs their substrate sets. AurKB has been
123 previously suggested to phosphorylate CKAP2 during mitosis[19]. Therefore, we sought to
124 determine if CKAP2 co-localizes with AurKA/B during mitosis. We employed RPE-1 cells with
125 GFP-CKAP2 knock-in[8], and stained for AurKA and AurKA phosphorylated on T288, which is a
126 requirement for and marker of AurKA activity[38,39]. This experiment revealed clear co-
127 localization of CKAP2 with AurKA and AurKA PT288 at centrosomes in prophase cells and
128 throughout mitosis. CKAP2 also substantially colocalized with AurKA and AurKA PT288 on
129 pole-proximal MTs during prometaphase and metaphase (Figure 2A). Consistently, CKAP2 also
130 largely colocalized with TPX2 on pole-proximal MTs during prometaphase and metaphase
131 (Figure 2B) in accordance with our CKAP2 interactome and immunoprecipitation data (Figure 1,
132 supplemental table 1). In contrast to AurKA/TPX2, which were present at spindle poles and
133 MTs, AurKB localized to centromeres during prophase-metaphase, and then changed localization
134 to the midbody during anaphase. CKAP2 did not co-localize with AurKB at any time during
135 mitosis (Figure S1B, S1C).

136 **AurKA/TPX2 phosphorylate CKAP2 during mitosis**

137 We next sought to determine if CKAP2 contains AurK consensus motifs. We identified
138 possible AurK phosphorylation sites at amino acids 39, 76, 209 and 347 (equivalent to mouse

139 CKAP2 sites 52, 86, 206 and 337) plus the sites in the c-terminus that had already been
140 identified[16–18]. The n-terminal phosphorylation sites are largely conserved in mammals, but not
141 other species (Figure 2C). We next examined previously published proteomic datasets to see if
142 phosphorylation of these sites has been previously detected. T209 phosphorylation has been
143 detected in previous studies, confirming that this site is phosphorylated in cells[21–23]. We next
144 examined the phosphorylation state of CKAP2 purified from mitotic cells. We
145 immunoprecipitated CKAP2 from Palbociclib-STLC synchronized RPE1 cell lysates. We boiled
146 the samples in the presence of SDS to avoid loss of CKAP2 in insoluble chromatin/MT fractions.
147 To determine if CKAP2 is phosphorylated in mitotic cells, we treated the immunoprecipitated
148 protein +/- lambda protein phosphatase before separation on SDS-PAGE. We then stained the gel
149 with ProQ Diamond to detect phosphorylated species and finally with Coomassie blue to
150 determine total protein levels. This experiment revealed that CKAP2 is phosphorylated in mitotic
151 cells as the phosphorylation signal disappears following treatment with lambda phosphatase
152 (Figure 2D). We then performed a similar experiment but treated the cells concurrently with
153 STLC and either DMSO solvent control or the AurKA inhibitor MLN8237 prior to harvesting the
154 cells. Interestingly, this experiment revealed a substantial loss of phosphorylation in MLN8237
155 treated cells, suggesting that AurKA is a key regulator of CKAP2 phosphorylation (Figure 2E)
156 during mitosis. Lastly, we tested if AurKA can phosphorylate CKAP2 *in vitro*. Therefore, we
157 incubated mouse CKAP2 together with purified GFP-Aurora A-6XHis and examined the
158 phosphorylation state of CKAP2 with ProQ Diamond stain. This experiment shows that AurKA
159 phosphorylates CKAP2 *in vitro* in an ATP and kinase-dependent manner (Figure 2F). Taken
160 together, these data demonstrate that CKAP2 colocalizes with, binds to and is phosphorylated by
161 AurKA/TPX2 during mitosis.

162 We next asked which protein phosphatase might antagonize CKAP2 phosphorylation by
163 AurKA. Obvious candidates to regulate CKAP2 include the PP1 and PP2A phosphatases.
164 Okadaic acid inhibits PP2A and PP1 to a lesser, though considerable extent[40,41]. Therefore, we
165 treated RPE1 cells with okadaic acid to see if it would affect the extent of CKAP2 binding to
166 MTs in mitotic cells. Although Okadaic acid treatment had a drastic effect on mitotic spindle
167 morphology owing to hyperstable kinetochore-MT attachments, CKAP2 remained bound to the
168 mitotic spindle to a similar extent both Okadaic acid and DMSO control treated cells (Figure
169 S2A, S2B). We also tested if Okadaic acid treatment directly affected the extent of CKAP2
170 phosphorylation during mitosis. Therefore, we synchronized RPE1 cells by sequential
171 Palbociclib-STLC synchronization and treated the cells with Okadaic acid or DMSO control for
172 2 hours prior to harvesting the cells. We then immunoprecipitated CKAP2 and measured the
173 change in CKAP2 phosphorylation using the phosphospecific ProQ Diamond stain. Okadaic acid
174 did not strongly affect the extent of CKAP2 phosphorylation (Figure S2C), consistent with the
175 lack of effect on CKAP2 binding to the mitotic spindle. Therefore, it is not likely that PP1 or
176 PP2A are the main phosphatase regulators of CKAP2 phosphorylation during mitosis.

177 **CKAP2 phosphorylation affects MT binding**

178 Phosphorylation is known to affect the ability of many MAPs to bind to MTs because it
179 carries a negative charge that repels similarly charged areas on MTs. For example, the protein
180 Hec1 is phosphorylated on up to 10 sites to control its affinity for MTs[42–45]. Therefore, we sought
181 to determine if phosphorylation of CKAP2 by AurKA affects its ability to bind MTs. We treated
182 RPE1 cells with 200 nM MLN8237 and examined the extent of CKAP2 overlap with the mitotic
183 spindle. This experiment revealed a substantial increase in signal overlap between CKAP2 and
184 the spindle in cells treated with the Aurora A inhibitor. Although the intensity ofCKAP2 staining

185 did not strongly change in treated cells, the intensity of β-tubulin staining was strongly
186 decreased, resulting in a normalized increase in CKAP2 binding to the spindle (Figure 3A-E).
187 We next tested if CKAP2 phosphorylation directly affects its ability to bind to MTs using
188 Total Internal Reflection Microscopy (TIRF) to visualize MTs and bound proteins. We again
189 incubated mouse CKAP2 together with AurKA +/- ATP to generate phosphorylated or sham
190 phosphorylated CKAP2. Then, we mixed these proteins with guanylylmethylene diphosphonate
191 (GMPCPP) MT seeds and taxol-stabilized MTs to determine if phosphorylation of CKAP2
192 affects its ability to bind to MTs *in vitro*. Interestingly, CKAP2 that had been phosphorylated by
193 AurKA was profoundly defective in binding microtubules *in vitro*. At 5 nM CKAP2, binding of
194 unphosphorylated CKAP2 to MTs was visible, but no binding of phosphorylated CKAP2 was
195 detectable. However, at 50 nM concentration, some binding of phosphorylated CKAP2 to MTs
196 was detectable, albeit at a much lower level than unphosphorylated CKAP2 (Figure 3F, 3G).
197 Taken together, our data indicate that phosphorylation of CKAP2 controls its affinity for MT
198 binding.
199 **TPX2 contributes to CKAP2 phosphorylation**
200 Since we detected CKAP2 in complex with TPX2 (Figure 1C-E, S1A), we next asked if
201 CKAP2 contributes to TPX2 localization to the mitotic spindle. Therefore, we compared the
202 intensity of TPX2 on the mitotic spindle in CKAP2-knockout[8] compared to Wild-type RPE1
203 cells. This experiment revealed a decrease in TPX2 on the mitotic spindle in 2 out of 3 clones of
204 CKAP2 knockout cells, while the third clone trended downwards in TPX2 intensity (Figure 4A,
205 4B). All 3 CKAP2 KO clones displayed less intense tubulin staining (Figure 4A, 4C). Therefore,
206 it is possible that CKAP2 either directly contributes to TPX2 levels on the spindle, or that the

207 low tubulin levels reduce TPX2 levels on the spindle since there are fewer MTs available for
208 TPX2 to bind to.

209 Our immunoprecipitation data suggest that CKAP2 binds directly to TPX2 and indirectly
210 to AurKA as we detected more TPX2 peptides by mass spectrometry, and we detected relatively
211 more TPX2 compared to Aurora A by Western blot. Therefore, we asked if the presence of TPX2
212 would enhance the phosphorylation of CKAP2 by Aurora Kinase A by functioning as a binding
213 intermediate between AurKA and CKAP2. We repeated our kinase assay in the presence or
214 absence of TPX2. Interestingly, the presence of TPX2 resulted in a clear increase in the amount
215 of CKAP2 phosphorylation by AurKA compared to CKAP2 incubated with AurKA alone (Figure
216 4D). In this assay, TPX2 was also robustly phosphorylated by AurKA.

217 To Determine how TPX2 and CKAP2 interact, we tested the ability of CKAP2 fragments
218 to pull down TPX2 and AurKA. CKAP2 was divided into four fragments: the N-terminal alpha-
219 helical domain (1-60), disordered domain (346-549), alpha-helical bundle (346-549) and C-
220 terminus (550-664)[46]. Interestingly, the disordered domain interacted robustly with TPX2 and
221 AurKA, and the N-terminal alpha-helical and C-terminal domains contributed to a lesser extent.
222 The alpha-helical bundle region of mmCKAP2 did not interact at all with TPX2 and AurKA
223 (Figure 4E). We then performed an Alphafold2[47] binding simulation between mmCKAP2 and
224 TPX2. Consistent with our pull-down experiment, Alphafold2 predicted that the basic residues of
225 the N-terminal alpha-helix, some residues within the disordered domain and a combination of
226 basic and acidic residues in the C-terminal domain all interact with TPX2 (Figure 4F).

227 **CKAP2 phosphorylation controls mitotic spindle growth**

228 To determine if phosphorylation of CKAP2 affects mitotic spindle functions, we
229 transfected RPE1 CKAP2 knockout cells with wild-type, phospho-null or phospho-mimic

230 mutants and measured the intensity of β-tubulin in STLC arrested cells with monopolar spindles.
231 In constructs containing a phospho-mimic mutation, all other potential phosphorylation sites
232 were mutated to alanine. Interestingly, cells expressing a phospho-null CKAP2 mutant displayed
233 slightly higher tubulin intensity. In contrast, cells expressing individual site phosphomimic
234 mutants displayed slightly lower tubulin staining, suggesting that phosphorylation of CKAP2 is
235 important for controlling its MT growth functions (Figure 5A, 5B). We also measured the
236 spindle diameter of STLC-arrested cells expressing the same mutants. Although in general the
237 spindle diameter was not strongly changed, cells expressing a CKAP2 mutant with all five
238 potential sites mutated to mimic phosphorylation, as well as individual site phosphomimic
239 mutants for T86 or T206, showed somewhat smaller mitotic spindle diameter (Figure 5A, 5C).
240 We next examined TPX2 and AurKA expression in cells expressing CKAP2 phospho-
241 null or phospho-mimic mutants. Several mutants showed decreased presence of TPX2 on the
242 mitotic spindle, including the 5A, 5D, 3D and S192 and T206 individual phospho-mimic sites
243 (Figure S3A, S3C), suggesting that either the reduced MT stability seen in cells expressing these
244 mutants affects TPX2 binding or perhaps that expression of these mutants directly affects TPX2
245 spindle binding. We also measured the intensity of AurKA on the mitotic spindle in cells
246 expressing our set of mutants. Unfortunately, our AurKA measurements showed numerous
247 outliers in one experimental replicate, resulting in inconclusive results. However, cells
248 expressing the S192 and T206 individual phospho-mimic proteins trended towards lower AurKA
249 levels on the mitotic spindle, which would be consistent with the TPX2 measurements (Figure
250 S3B, S3D). Taken together, these data suggest that CKAP2 phosphorylation affects the stability
251 of the mitotic spindle and AurKA/TPX2 activity.

252 Since CKAP2 contributes to TPX2 spindle localization, we considered the possibility that
253 TPX2 and CKAP2 might function together to regulate MT growth. Therefore, we analysed how
254 TPX2 and CKAP2 contribute to microtubule dynamics individually and together in an *in vitro*
255 MT growth assay. In the absence of CKAP2 and TPX2 we observed MT growth and occasional
256 depolymerization. As shown previously, 50 nM CKAP2 potently increased microtubule growth
257 rates and suppressed MT catastrophe[9]. Also as shown previously, 50 nM TPX2 suppressed MT
258 off-rates when applied alone[34]. When applied together, the effect of CKAP2 was dominant since
259 it prevented catastrophe events, masking the ability of TPX2 to suppress MT off-rates. No
260 synergistic effects were observed between CKAP2 and TPX2, as MT dynamics were similar
261 between the CKAP2 only and CKAP2 plus TPX2 conditions (Figure 5D, 5E).

262 **CKAP2 phosphorylation dynamics are required for cell viability**

263 We next sought to determine how CKAP2 phosphorylation is important for mitotic
264 progression and cell viability. Although we were unable to use puromycin to select for RPE1
265 cells expressing wild-type or AurKA site mutants of CKAP2, we were able to do so for cancer
266 cell lines. Therefore, we transfected HeLa cells with either empty vector expressing mNeon
267 Green, CKAP2 wild-type, or CKAP2 AurKA site mutants fused to mNeon Green. We then added
268 puromycin selection, incubated for 12 days and finally fixed and stained the cells with crystal
269 violet to assess colony formation. Transfection of the empty vector supported robust colony
270 formation, as did transfection of CKAP2 wild-type. Interestingly, a phospho-null mutant (5A)
271 supported viability to a similar extent as CKAP2 wild-type. A mutant containing T86E, S192D
272 and T206E (3E) and the single mutants T52E and T86E also supported cell viability to a similar
273 extent as CKAP2 wild type. The construct containing T52E, T86E, S192D, T206E and T337E
274 (5E), T52E and T337E (2E) and the single site mutants S192D and T206E poorly supported

275 colony formation, suggesting that CKAP2 phosphorylation dynamics are important for
276 supporting cell viability (Figure 5F). Consistently, these two mutants single site mutants S192D
277 and T206E also had substantially diminished spindle microtubule density in mitotic cells (Figure
278 5A, 5B).

279 **Discussion**

280 Using unbiased proteomics, we have discovered numerous proteins that interact with
281 CKAP2 during mitosis (Figure1, supplemental table 1). Interestingly, most of these proteins are
282 not obviously components of the mitotic spindle or MAPs, despite the obvious spindle
283 localization of CKAP2 during mitosis. Thus, it is likely that CKAP2 has other roles during
284 mitosis, or alternatively that the interacting proteins have uncharacterized spindle roles in
285 mitosis. However, many of these proteins, such as the cohesins and condensins, could potentially
286 serve as receptors for CKAP2 to bind to chromatin in late mitosis. Importantly, AurKA/TPX2
287 were the only mitotic kinase or phosphatase that we detected in our screen despite the fact that
288 phosphatase regulation of proteins is essential to dampen kinase activity, and Cdk
289 phosphorylation has already been shown to regulate CKAP2, consistent with the presence of
290 multiple potential proline-directed phosphorylation sites in the C-terminus[16–18].

291 We envision a model for CKAP2 function where AurKA/TPX2 phosphorylates CKAP2
292 in response to cues from the spindle state to constrain mitotic spindle growth as part of a
293 negative feedback loop. CKAP2 is an extremely potent nucleator and stabilizer of MTs, and so
294 logically, such a protein would require a negative regulator to dampen its activity to prevent
295 unrestrained spindle growth. Since phosphorylation adds a negative charge to proteins, this
296 would cause a reduction in binding affinity of CKAP2 for MTs that would result in a reduction in
297 MT polymerization activity (Figure 3, Figure 6). In this scenario, AurKA/TPX2 kinase activity

298 would cause spindle growth, which would in turn allow more binding of AurKA/TPX2 to the
299 spindle, resulting in more kinase activity and increased CKAP2 phosphorylation, which will then
300 start to dampen spindle growth.

301 Although the structure of CKAP2 bound to MTs has not yet been solved, the structure of
302 TPX2 bound to MTs has been determined. Unlike CKAP2, which binds to MTs both during
303 interphase and mitosis, TPX2 only binds to MTs during mitosis[28]. TPX2 uses two linked regions
304 to bind across both longitudinal and lateral MT interfaces[29]. It will be interesting to compare and
305 contrast the binding mode of CKAP2 to MTs to determine if it competes with TPX2, binds to an
306 independent site or synergizes with TPX2 for MT binding. However, in terms of activity, CKAP2
307 appears to directly facilitate MT growth, whereas TPX2 largely reduces MT disassembly rates by
308 slowing the MT-off -rate. Thus, CKAP2 and TPX2 perform different roles in promoting MT
309 growth and stability. Importantly, the n-terminus of CKAP2 is largely disordered, and so it might
310 be able to bind MTs in multiple conformations, which could be impacted by phosphorylation.
311 The disorder of CKAP2 also likely contributes to the ability of AurKA/TPX2 to phosphorylate
312 CKAP2. We found that it is largely the disordered domain of CKAP2 which binds to TPX2
313 (Figure 4E). We speculate that this would position CKAP2 in such a way that the N-terminal
314 disordered domain of CKAP2 can be optimally phosphorylated by AurKA, as we found
315 substantially enhanced phosphorylation of CKAP2 in the presence of TPX2 and AurKA
316 compared to AurKA alone (Figure 4D).

317 We identified up to 5 AurKA phosphorylation sites in the N-terminus of mouse CKAP2
318 and 4 in human CKAP2. Of these, the most ideal consensus motif based on the amino acid
319 sequence is in T39 (mouse T52). However, this site is located within an alpha-helix and might
320 not be accessible to the kinase. This site has previously been identified in a screen for AurKB

321 substrates, but not directly in cell lysates[48]. This experiment was performed by mixing lysate
322 with purified kinase, which might allow the kinase to encounter substrates that it might not
323 normally encounter due to the lack of spatial organization present in a lysate. Although it is not
324 inconceivable that soluble CKAP2 might encounter soluble AurKB, considering that the bulk of
325 these proteins are localized to different structures (Figure S1B, S1C), it is unlikely that AurKB
326 can substantially phosphorylate CKAP2. In contrast, since AurKA/TPX2 binds to CKAP2 as
327 detected by MS and Western blot and largely co-localizes throughout mitosis; it is much more
328 likely that CKAP2 is regulated by AurKA. Human CKAP2 T76 phosphorylation (mouse T86)
329 has not yet been detected directly, despite forming a good AurK consensus site in an unstructured
330 region. Human CKAP2 S190 phosphorylation has been detected. However, it is unclear which
331 kinase might phosphorylate it. Human CKAP2 S209 (mouse T206) has also been detected and
332 forms a good AurK consensus site. Consistently, our cell biology and *in vitro* experiments point
333 to the T206 phosphorylation site being the most important one for regulating CKAP2 functions.
334 Cells expressing this mutant have substantially less stable MTs compared to cells expressing
335 wild-type CKAP2 and mutation of this site does not efficiently support cell viability (Figure 5A,
336 5B, 5F). Future studies will aim to determine exactly how phosphorylation of this site impairs
337 the ability of CKAP2 to bind MTs and stimulate their growth.
338 Overall, our study provides a valuable resource for further investigation of CKAP2 and
339 the cellular pathways in which it participates. Future studies will be necessary to validate the
340 binding of the other proteins we detected and to determine their contributions to the functions of
341 CKAP2 in mitosis and interphase.
342 **Resource availability**

343 The cell biology datasets generated during and/or analysed during the current study are available
344 from the corresponding author on reasonable request. The original datasets for CKAP2
345 interactome has been deposited to the ProteomeXchange Consortium via the PRIDE[49] partner
346 repository with the dataset identifiers to be determined following acceptance of the article for
347 publication.

348 **Acknowledgements**

349 We thank Arnold Hayer and Jose Teodoro for providing reagents. We thank Denis Faubert and
350 Josée Champagne for assistance with the proteomics analysis. We also thank members of the
351 Bechstedt laboratory and Gary Brouhard for helpful suggestions and feedback. The laboratory of
352 SB is supported by grants from the Canadian Institutes of Health Research (CIHR PJT-189995),
353 the Natural Sciences and Engineering Research Council of Canada (NSERC; RGPIN-2024-
354 05603), and in part by a Fonds de Recherche du Québec (Health Sector) Research Centres Grant
355 #288558.

356 **Author Contributions**

357 Conceptualization: SB and TJK. Investigation: TJK, TL. Formal analysis: TJK, TL.
358 Methodology: TJK, SB. Funding acquisition: SB. Supervision: SB. Writing- original draft: TJK,
359 SB. Writing- review & editing: TJK, SB. Project administration: SB.

360 **Declaration of interests**

361 The authors declare that they have no conflicts of interest

362 **Materials and Methods**

363 <u>Cell Culture</u>

364 RPE1 were a gift from Arnold Hayer (McGill University). RPE1 CKAP2 GFP-CKAP2 and
365 CKAP2 knockout cells were described previously[8]. All cells were grown at 37°C in a humidified

366 environment with 5% CO_2. HeLa cells and U20S cells were purchased from the ATCC and
367 grown in Dulbecco's modified Eagle medium (Life Technologies #11995073) containing 10%
368 Fetal bovine serum (Wisent #098150), 50 U/mL penicillin and 50 µg/mL streptomycin (Life
369 Technologies #15140122). RPE1 cells were grown in DMEM-F12 (Life Technologies
370 #11320082) with the same supplements. Cells were verified to be free of mycoplasma by
371 frequent staining of plated cells with DAPI. No contamination was observed.

372 Inhibitors and reagents

373 STLC (Fisher Scientific #T25225G) was used at 25 µM. Okadaic acid (Cell Signaling
374 Technology #5934) was used at 100 nM. MLN8237 (Selleck #1028486-01-2) was used at 25-500
375 nM. Palbociclib (MilliporeSigma #PZ0383-5MG) was used at 1 µM. Taxol (Fisher Scientific
376 #AAJ62734MC) was used at varying concentrations. Puromycin (BioBasic # PJ593) was used at
377 1 µg/ml.

378 Plasmids and cloning

379 Mouse CKAP2 and codon optimized mouse TPX2 were cloned into pHAT His-USER-GFP-Strep
380 via USER cloning[50]. It was also cloned into pTWIST Puro EF1alpha-USER-mNeonGreen via
381 USER cloning. Aurora A site mutants of mouse CKAP2 were created by custom DNA synthesis
382 by Twist Bio and then cloned into plasmids via USER cloning[50]. mmCKAP2 fragments were
383 described previously[46]. The DNA constructs were then verified by Sanger sequencing.

384 Transfections

385 RPE1 or HeLa cells were transfected using Xfect™ transfection reagent (Takara Bio #631318)
386 according to the manufacturer's directions. Briefly, media on the cells was changed for 500 µl
387 for a 12-well plate. 4 µg of DNA was mixed with 100 µl of buffer. 1.2 µl of Xfect reagent was

388 then added, and the solution mixed by vortex. After 5 minutes incubation, 50 µl of transfection
389 mix was added to cells overnight. The media was then changed 24 hours later.

390 Immunofluorescence

391 Following treatments, cells were fixed in 4% paraformaldehyde in PBS at room temperature for
392 20 minutes. The cells were washed twice with PBS and then permeabilized in PHEM buffer (60
393 mM PIPES, 25 mM HEPES, pH 6.9, 10 mM EGTA, and 4 mM $MgSO_4$, 1% Triton X-100, 10
394 mM glycerol 2-phosphate) for 10 minutes. The cells were then washed twice with PBS for before
395 blocking with ADB (10% serum, 0.1% Triton X-100 in PBS) for 15 minutes. Primary antibodies
396 were then diluted in ADB and used at the indicated dilution. Secondary antibodies were diluted
397 in ADB. After incubation with antibodies, the cells were washed three times with PBS 0.1%
398 Triton X-100. Finally, the cells were counterstained with DAPI and mounted on slides using
399 FluorSave™ antifade reagent (Millipore #345789-20 ml).

400 Immunoprecipitation

401 For protein-protein interactions, 500,000 RPE1 cells were plated on 10 cm dishes (5 per
402 condition). 24 hours later, palbociclib was added. 18 hours following palbociclib addition, it was
403 washed out with 2 4 ml washes with PBS. STLC was then added 5 hours later. 20 hours post-
404 release, the cells were harvested by scraping, washed once with cold PBS, and lysed in the
405 following buffer: 0.5% NP40, 100 mM NaCl, 50 mM tris pH 7.4, 10 mM glycerol 2-phosphate.
406 Cells were lysed on ice for 20 minutes before centrifuging at 15,000 x g for 20 minutes at 4ºC.
407 The supernatant was transferred to a fresh tube, and input sample set aside. 10 µl of packed
408 volume protein G beads were added to each sample together with 5 µg of antibody for 2 hours on
409 a rotating platform at 4ºC. The beads were then washed 5 times in lysis buffer and dried using a

410 30 g needle attached to a vacuum line. 30-100 µl of 1X sample buffer were added to the beads
411 before elution by boiling and loading on gel.
412 For phosphorylation analysis, cells were prepared and synchronized as above. Following
413 harvesting, the cells were lysed in 50 mM Tris pH 7.5 and 1% SDS. The lysates were then boiled
414 for 5 minutes. SDS was then inactivated by 10-fold dilution with 1.5% Triton X-100 in TBS.
415 Debris was then pelleted via centrifugation at 15,000 x g for 20 minutes at 4ºC. CKAP2 was then
416 immunoprecipitated using anti-CKAP2 and protein G agarose as above.
417 Mass Spectrometry
418 CKAP2 was purified from palbociclib-STLC synchronized cells by immunoprecipitation as
419 described above. The entire reaction was then eluted in sample buffer and separated on a 10%
420 SDS-PAGE gel. The gel was then stained with Coomassie blue, and each lane was cut into 12
421 slices. Gel bands were excised under a clean bench and cut into 1 mm^3 pieces. For all subsequent
422 steps, reagent volumes were adjusted according to the volume of the gel pieces. Gel pieces were
423 first washed with water for 5 minutes, then destained twice using a destaining buffer composed
424 of 50 mM ammonium bicarbonate and 50 µL of acetonitrile, each for 10 minutes. Following this,
425 the gel pieces were dehydrated with acetonitrile. Proteins were reduced by incubating the gel
426 pieces in reduction buffer (10 mM DTT, 100 mM ammonium bicarbonate) for 30 minutes at
427 40 °C, and subsequently alkylated with alkylation buffer (55 mM iodoacetamide, 100 mM
428 ammonium bicarbonate) for 20 minutes at 40 °C in the dark. The gel pieces were then
429 dehydrated and washed at 40 °C with acetonitrile for 5 minutes before removing all reagents.
430 They were dried for 5 minutes at 40 °C and then rehydrated at 4 °C for 40 minutes with trypsin
431 solution (6 ng/µL sequencing-grade trypsin from Promega in 25 mM ammonium bicarbonate).
432 The low concentration of trypsin was used to minimize signal suppression and background from

433 autolysis products during LC-MS/MS analysis. Protein digestion was carried out at 58 °C for 1
434 hour and quenched with 15 µL of 1% formic acid / 2% acetonitrile. The supernatant was
435 transferred to a 96-well plate. Peptide extraction was performed in two 30-minute steps at room
436 temperature using an extraction buffer (1% formic acid / 50% acetonitrile). All peptide extracts
437 were completely dried using a vacuum centrifuge. The LC column used was a PicoFrit fused
438 silica capillary column (15 cm × 75 µm i.d.; New Objective, Woburn, MA), self-packed with
439 C18 reversed-phase material (Jupiter, 5 µm particles, 300 Å pore size; Phenomenex, Torrance,
440 CA) using a high-pressure packing cell. This column was installed on the Easy-nLC II system
441 (Proxeon Biosystems, Odense, Denmark) and coupled to a Q Exactive mass spectrometer
442 (ThermoFisher Scientific, Bremen, Germany) equipped with a Proxeon nanoelectrospray Flex
443 ion source. The chromatography buffers were 0.2% formic acid in water (buffer A) and 100%
444 acetonitrile with 0.2% formic acid (buffer B). Peptides were loaded on-column and eluted using
445 a three-step gradient at a flow rate of 250 nL/min. Solvent B increased from 2% to 35% over 15
446 minutes, then from 35% to 50% over 7 minutes, and finally from 50% to 90% over 5 minutes.
447 LC-MS/MS data were acquired using a data-dependent Top12 method combined with a dynamic
448 exclusion window of 7 seconds. The mass resolution for full MS scans was set to 70,000 (at m/z
449 400), and lock masses were used to improve mass accuracy. The mass range for MS scanning
450 was from 360 to 2000 m/z, with a target value of 1×10^6 and a maximum ion fill time of 100 ms.
451 Data-dependent MS2 scan events were acquired at a resolution of 17,500, with a maximum ion
452 fill time of 50 ms, a target value of 1×10^5, an intensity threshold of 1.0×10^4, and an underfill
453 ratio of 0.5%. The normalized collision energy was set to 27%, and the capillary temperature was
454 maintained at 250 ºC. Nanospray and S-lens voltages were set to 1.3–1.7 kV and 50 V,
455 respectively. Protein database searches were performed using Mascot 2.6 (Matrix Science)

456 against the UniProt human database. The mass tolerance was set to 10 ppm for precursor ions
457 and 0.5 Da for fragment ions. Trypsin was specified as the enzyme, allowing up to two missed
458 cleavages. Carbamidomethylation of cysteine was set as a fixed modification, and methionine
459 oxidation was included as a variable modification.

460 SDS-PAGE and Western blot

461 Gels and blots were performed as described previously [51]. Prior to loading samples on gel, 4X
462 Laemmli buffer (200 mM Tris pH 6.8, 4% SDS, 40% glycerol, 4% 2-mercaptoethanol, 0.12
463 mg/ml bromophenol blue) was added to a final dilution of 1X, and the samples were boiled for 5
464 minutes. Proteins were separated on SDS-PAGE gel using stacking gel (4% 29:1 acrylamide:
465 Bis-acrylamide, 125mM Tris pH 6.8, 0.1% SDS, 0.1% ammonium persulfate, 0.1% TEMED)
466 and (8-15% 29:1 acrylamide: Bis-acrylamide, 400 mM Tris pH 8.8, 0.1% SDS, 0.1% ammonium
467 persulfate, 0.1% TEMED) at 120V until the bromophenol blue has run off or longer, as needed.
468 Transfer onto nitrocellulose membrane was performed for at least 24 hours at 30V under wet
469 conditions in 1X transfer buffer (14.4 g/L glycine, 3.0 g/L Tris, 20% methanol). Conditions for
470 western blots includes the use of 5% nonfat dry milk in TBS-T 0.5% (50 mM Tris [pH 7.2], 150
471 mM NaCl, 0.5% Tween 20) for blocking and TBS-T 0.5% for washing. 4 washes for 10 minutes
472 each were performed after primary and secondary antibody incubation periods. The bands were
473 visualized by enhanced chemiluminescence using Clarity (Bio-Rad #1705060) using a Bio-Rad
474 ChemiDoc™ Touch Imaging System.

475 *In vitro* analysis of CKAP2

476 Mouse CKAP2 protein variants were produced in the E. Coli strain BL21. The bacteria were
477 suspended in in 25 ml buffer A (50 mM $NaPO_4$, 10 mM Imidazole, 300 mM NaCl, 10%
478 Glycerol, pH 8) and processed in an emulsiflex high-pressure homogenizer (Avestin). The lysate

479 was then ultracentrifuged at 45Ti rotor at 25000 RPM for 45 minutes. 200 µl of packed
480 glutathione agarose was then added for 2 hours on a rotating platform. 1 ml Ni-NTA agarose was
481 then added to the lysate for 2 hours on a rotating platform. The agarose was then washed, and
482 purified proteins eluted with buffer A containing 300mM imidazole and then dialyzed against
483 0.4X TBS. Glycerol was then added to 10% and the proteins frozen until further use. Kinase
484 reactions were performed by mixing CKAP2, GFP-Aurora A-6XHis, 100 µM ATP in kinase
485 buffer 50 mM Tris pH 7.2, 25 mM NaCl, 10mM $MgCl_2$ 1mM DTT, 0.01% Triton X-100 for 1
486 hour at 37ºC. The reactions were stopped by addition of 4X SDS sample buffer, and half the
487 reaction loaded on SDS-PAGE gel. The gels were then stained with ProQ Diamond
488 phosphoprotein stain (Thermo Scientific) according to the manufacturer's instructions and
489 subsequently with Coomassie blue.
490 *In vitro* MT assays were performed as described previously[9]. CKAP2 fragments were produced
491 in BL21(DE3) *E. coli* grown in LB media to OD_{600} and then induced with 0.5 mM Isopropyl-D-
492 1-thiogalactopyranoside (IPTG) at 20ºC overnight. The bacteria were then harvested and lysed in
493 Buffer A (50 mM NaH2PO4, 300 mM NaCl, 0 mM imidazole, pH 7.8) using an EmulsiFlex-C5
494 (Avestin Inc, Canada). Debris was then pelleted by ultracentrifugation at 30,000 x g for 1 hour at
495 4ºC. The lysate was then loaded onto a column containing His60 Ni SuperFlow Resin (Takara
496 Bio, USA). Purified protein was eluted with Buffer B (50 mM NaH2PO4, 300 mM NaCl, 200
497 mM imidazole, pH 7.8). Eluted proteins were then loaded onto a column containing Strep-Tactin
498 Sepharose resin (IBA Lifesciences, Germany), washed with 5 column volumes of Buffer W (100
499 mM Tris-HCl, 150 mM NaCl, 1 mM EDTA, pH 7.8) and finally eluted with Buffer W
500 supplemented with 2.5 mM Desthiobiotin. Protein concentration was determined by measuring
501 the absorbance at 280 or 488 nm using a DS- 11 FX spectrophotometer (DeNovix Inc, USA).

502 SDS-PAGE was used to determine the purity of the proteins. Tubulin was purified from bovine
503 brains as previously described[52] with the difference of having used Fractogel EMD SO3- (M)
504 resin (Millipore-Sigma) instead of phosphocellulose. Tubulin was labelled using CF640R-NHS-
505 Ester (Biotium, USA) and tetramethylrhodamine (TAMRA, Invitrogen Inc, Canada), as
506 previously described[53]. Before use, an additional cycle of MT polymerization was performed.
507 Microscope Slide Channel Preparation
508 Glass coverslips (22x22 and 18x18 mm) were washed with acetone and then sonicated in 50%
509 methanol with 0.5 M KOH and finally rinsed with water. The coverslips were then dried and
510 exposed to air plasma (Plasma Etch) for 3 minutes before silanizing by soaking them in 0.1%
511 dichlorodimethylsilane in *n*-heptane before sonicating them in *n*-heptane and finally in ethanol.
512 Flow channels with a volume of 7 µl were created by using two pieces of silanized coverslips
513 held by double-sided tape in custom coverslip holders. The channels were incubated with anti-
514 TAMRA antibodies for 5 minutes, blocked with 5% Pluronic F-127 for 10 minutes and washed
515 with BRB80 before incubation with MTs. The channels were used at 35ºC using a heated
516 microscope objective and incubation chamber.
517 Binding to Paclitaxel-stabilized MTs
518 GDP-MTs stabilized by paclitaxel were prepared by polymerizing a 1:15 ratio of TAMRA-
519 labelled to unlabeled tubulin in the presence of 4 mM $MgCl_2$, 1mM GTP, 5% DMSO in BRB80
520 buffer. The mixture was then incubated for 30 minutes at 37ºC. The MTs were then diluted using
521 BRB80 plus 10 µM paclitaxel, pelleted at 100,000 RPM at 30 psi for 7 minutes using an Airfuge
522 (Beckman-Coulter) and finally resuspended in BRB80 plus µM paclitaxel.
523 To assess binding of CKAP2 to MTs, A combination of GMPCPP double-cycled MTs and
524 paclitaxel-stabilized MTs were mixed and flowed into microscope slide channels. Since the

525 paclitaxel-stabilized MTs contain less TAMRA label, they possess a dimmer signal compared to
526 GMPCPP MTs.

527 Dynamic Microtubule Assay

528 GMPCPP MT seeds were created by polymerizing a 1:4 ratio of TAMRA-labelled to unlabeled
529 tubulin in the presence of 1 mM guanosine-5'- [(α, β)-methyleno] triphosphate (GMPCPP, Jena
530 Biosciences, Germany), a non-hydrolyzable GTP analogue during two cycles. On the day of an
531 experiment, unlabeled and CF642R-labeled tubulin were mixed at a 1:17 ratio, aliquoted and
532 flash-frozen in liquid nitrogen. To start an experiment, GMPCPP MT seeds were flowed into a
533 channel and then washed with BRB80 buffer. MT growth was initiated by introducing tubulin (8
534 μM) in BRB80 buffer containing 1 mM GTP, 40 mM D-glucose, 64 nM catalase, 250 nM
535 glucose oxidase, 10 mM DTT, 0.1 mg/ml BSA together with CKAP2. Images were then taken at
536 suitable time points to track MT growth and catastrophe.

537 Colony formation assays

538 300, 000 HeLa cells per well were plated on 6-well plates. 24 hours following plating, the cells
539 were transfected overnight as described above. 18 hours following transfection, the media was
540 changed. 42 hours following transfection, the media was changed to include puromycin selection
541 (1 μg/ml) for 3 days. The media was then changed for media containing 0.2 μg/ml puromycin,
542 and the cells were allowed to proliferate for another 12 days before fixation and staining with
543 crystal violet.

544 Microscopy

545 Images were acquired with either a Zeiss Axio Observer 7 fitted with a TIRF
546 equipped with a Prime 95B CMOS camera (Photometrics) with a pixel size of 107 nm controlled
547 by Zeiss Zen 2.5 Blue Edition software version or a Nikon Eclipse Ti microscope spinning disc

548 confocal (Cicero; Crest Optics) microscope equipped with AURA III Light Engine (Lumencor®)
549 and Hamamatsu ORCA-fusion C14440 camera with 110 nm pixel size controlled by Nikon-
550 Elements AR 6.10.01 software. Images were acquired in 0.15-0.4 μm sections using a plan apo
551 1.4 numerical aperture 100X or 60X oil-immersion objective using 1X1 binning. All image
552 analysis, adjustments, measurements and cropping were performed using Fiji software [54].
553 Widefield Image deconvolution was performed using Zen Blue Edition 2.5 software. All protein
554 intensity analysis was performed on the raw images. Line scans were performed on the
555 deconvoluted images in Fiji and the data was then exported to Graphpad Prism version 8.4.3. or
556 version 10.2.1

557 Antibodies

558 The following antibodies were used for immunofluorescence (IF) and/or immunoblotting (IB):
559 mouse anti-Aurora A (Cell Signaling Technology 1F8; IF at1:1000, blot at 1:500), Rabbit anti-
560 Aurora A pT288 (Cell Signaling Technology C39D8; IF at 1:500), mouse anti-TPX2 (Cell
561 Signaling Technology D9Y1V; IF at 1:1000, blot at 1:500), rabbit anti-Aurora B (Cell Signaling
562 Technology 3094T; IF at 1:50), mouse anti-β–Tubulin (Sigma clone 2.1 T4026; IF at 1:200),
563 rabbit anti-CKAP2 (Proteintech 25486-1-AP; blot at 1:500), Rabbit anti-CKAP2 (AbClonal
564 A9706; IF at 1:200), Mouse anti-TAMRA (Invitrogen 5G5; label at 1:100). Secondary antibodies
565 used were highly cross-adsorbed Alexa Fluor® 488, 594 and 647 raised in donkey or goat
566 (Invitrogen; IF at 1:1000), horseradish peroxidase (Bio-Rad; IB at 1:10000-10,0000), Anti-IgG
567 (H+L) Goat Polyclonal Antibody (Horseradish Peroxidase), Peroxidase AffiniPure Goat Anti-
568 Rabbit IgG (H+L) (IB at 1:5000), Goat Polyclonal Antibody (Horseradish Peroxidase),
569 Peroxidase AffiniPure Goat Anti-Mouse IgG (H+L) (IB at 1:5000).

570 Statistical analysis of cell biology and MT data

571 All statistical tests were performed using Graphpad Prism version 8.4.2. Except where indicated,
572 all experiments were performed as 2-3 independent biological repeats. In most IF experiments,
573 25 cells for each condition were measured. Experiments with other numbers are noted in the
574 figure legends.

575 **Figure legends**

576 **Figure 1: Proteomic screening identifies AurKA/TPX2 as CKAP2 interacting proteins**

577 A) Cartoon diagram showing the experimental scheme for determining CKAP2 binding
578 partners. RPE1 cells were first synchronized in mitosis by Palbociclib-STLC block. The
579 cells were then harvested and lysed. Endogenous CKAP2 was then immunoprecipitated
580 from the mitotic lysate together with interacting proteins. The purified proteins were then
581 separated via SDS-PAGE. The gel lanes were then cut into 12 slices and analysed by
582 mass spectrometry to identify CKAP2 interaction partners. A single experiment was
583 performed.

584 B) Proteins from the phospho-proteomic screen from (A) that that met criteria of at least 4
585 peptides detected and 4:1 signal to noise ratio were analyzed for gene ontology. The data
586 were then transferred to Prism software and plotted.

587 C) STRING analysis of the proteins from (A) meeting detection criteria showing protein
588 interaction networks.

589 D) Selected interacting proteins detected in the control immunoprecipitation and CKAP2
590 immunoprecipitations from (A) showing the number of total detected peptides.

591 E) RPE1 cells were prepared as in panel (A), except that purified proteins were analyzed by
592 Western blot. CKAP2 was immunoprecipitated from Palbociclib-STLC mitotic lysates
593 and the purified proteins were then separated by SDS-PAGE, transferred to nitrocellulose

594 membrane and blotted as indicated. The panels were adjusted for brightness and contrast.
595 An experiment representative of two independent biological repeats is shown.
596
597 **Figure 2: CKAP2 co-localizes with and is phosphorylated by AurKA/TPX2**
598 A) Immunofluorescence images from RPE1 eGFP-CKAP2 cells in various stages of mitosis
599 stained for AurKA, AurKA pT288 and DAPI. The CKAP2-eGFP, AurKA and AurKA
600 pT288 channels were adjusted evenly for brightness and contrast. The DAPI channel of
601 each condition was adjusted independently. Representative images from 2 independent
602 biological experiments are shown. Scale bars, 10 μm and 1 μm (inset).
603 B) Immunofluorescence images from RPE1 eGFP-CKAP2 cells in various stages of mitosis
604 stained for TPX2 and DAPI. The CKAP2-eGFP and TPX2 channels were adjusted evenly
605 for brightness and contrast. The DAPI channel of each condition was adjusted
606 independently. Representative images from 2 independent biological experiments are
607 shown. Scale bars, 10 μm and 1 μm (inset).
608 C) Amino acid sequence alignment of CKAP2 orthologs showing predicted AurKA
609 phosphorylation consensus motifs. Residues highlighted in green indicate potential AurK
610 phospho-acceptor residues.
611 D) RPE1 cells were synchronized by Palbociclib-STLC block. The cells were then harvested
612 and lysed by boiling in SDS-containing buffer. The SDS was then inactivated by 10-fold
613 dilution with 1.5% Triton X-100 buffer. CKAP2 was then purified by
614 immunoprecipitation. The protein-G agarose beads were either sham treated or treated
615 with Lambda protein phosphatase for 30 minutes at 30ºC. The beads were then boiled in
616 sample buffer to elute purified proteins. Purified proteins were then separated by SDS-

617 PAGE, which was then stained with with ProQ Diamond phosphoprotein stain and
618 imaged. Finally, the gel was stained with Coomassie blue and imaged again. An
619 experiment representative of two independent biological repeats is shown.

620 E) Cells were prepared as in (D), except that one set of cells was treated concurrently with
621 STLC and DMSO control and one set with MLN 8237 AurKA inhibitor. CKAP2 was
622 then purified and analysed as in (D). An experiment representative of two independent
623 biological repeats is shown.

624 F) Purified GFP-Aurora A-6XHis and His-mmCKAP2-GFP-Strep were mixed with reaction
625 components as indicated and incubated at 37ºC for 1 hr. The reaction was then separated
626 by SDS-PAGE gel. The gel was then stained with ProQ Diamond phosphoprotein stain,
627 imaged and subsequently stained with Coomassie blue and re-imaged. An experiment
628 representative of two independent biological repeats is shown. High-brightness/contrast
629 and low-brightness/contrast images are shown for presentation.

630 **Figure 3: Phosphorylation the mitotic spindle localization of CKAP2**

631 A) Immunofluorescence images from asynchronous RPE1 cells in late prometaphase were
632 treated with either DMSO or MLN8237 for 3 hours and then fixed and stained for
633 CKAP2, β-tubulin and DAPI. The CKAP2 and β-tubulin channels were adjusted evenly
634 for brightness and contrast. The DAPI channel of each condition was adjusted
635 independently. Representative images from 2 independent biological experiments are
636 shown. Scale bars, 10 μm and 1 μm (inset).

637 B) Line scans across the indicated paths from the images in panel (A).

638 C) Quantification of the CKAP2-β-tubulin ratio from panel (A). The Z-section with the
639 brightest signal was chosen, and an outline traced around the mitotic spindle. The levels

640 of CKAP2 and β-tubulin were then measured. Background signal was taken as the
641 minimum measured value in the mitotic spindle area and subtracted from the measured
642 signal. At least 50 cells per condition for each of 3 independent biological repeats were
643 measured. Error bars indicate the mean +/- SEM. Statistical significance was calculated
644 between the indicated conditions using Student's T- test.

645 D) Quantification of the CKAP2 levels from panel (A) as for panel (C).

646 E) Quantification of the β-tubulin levels from panel (A) as for panel (C).

647 F) TIRF microscopy images of CKAP2 together with guanosine-5'[(α,β)-methleno]
648 triphosphate GMPCPP-seeds and paclitaxel-stabilized MTs. CKAP2 was incubated *in*
649 *vitro* with AurKA in the presence or absence of ATP. Channels in between silanized-glass
650 coverslips were prepared by flowing-in anti-TAMRA antibodies. After washing, TAMRA
651 labelled GMPCPP-seeds and paclitaxel-stabilized MTs were flowed-into the chamber.
652 Then, CKAP2 prepared as indicated was also flowed into the chamber and images were
653 taken. Representative images from 2 independent biological experiments are shown.
654 Scale bar, 5 μm.

655 G) Quantification of the results presented in (F). The fluorescence intensity of CKAP2 on
656 each of 20 GMPCPP seeds or 20 paclitaxel stabilized microtubules was quantified.

657 **Figure 4: TPX2 and CKAP2 reciprocally regulate their microtubule binding activities**

658 A) Immunofluorescence images of asynchronous RPE1 wild-type and CKAP2 KO clones 8,
659 9 and 12. The cells were plated on glass coverslips, allowed to proliferate and then fixed
660 and stained for TPX2, β–tubulin and DAPI. The CKAP2 and β-tubulin channels were
661 adjusted evenly for brightness and contrast. The DAPI channel of each condition was

662 adjusted independently. Representative images from 2 independent biological
663 experiments are shown. Scale bars, 10 μm.
664 B) Quantification of the TPX2 levels from panel (A). The Z-section with the brightest signal
665 was chosen, and an outline traced around the mitotic spindle. The levels of TPX2 were
666 then measured. Background signal was taken as the minimum measured value in the
667 mitotic spindle area and subtracted from the measured signal. At least 25 cells per
668 condition for each of 3 independent biological repeats were measured. Error bars indicate
669 the mean +/- SEM. Statistical significance was calculated between the indicated
670 conditions using Dunnett's multiple comparison test.
671 C) As for panel (B) but the β–tubulin levels quantified
672 D) Purified GFP-Aurora A-6XHis, His-mmTPX2-GFP-Strep and His-mmCKAP2-GFP-
673 Strep were mixed with reaction components as indicated and incubated at 37ºC for 1 hr.
674 The reaction was then separated by SDS-PAGE gel. The gel was then stained with ProQ
675 Diamond phosphoprotein stain, imaged and subsequently stained with Coomassie blue
676 and re-imaged. The images were adjusted for brightness and contrast for presentation. An
677 experiment representative of two independent biological repeats is shown.
678 E) His-mmCKAP2-GFP-Strep fragments were purified by one-step Strep affinity gel
679 purification. Concurrently, HeLa cells were synchronized by thymidine-nocodazole
680 block. The cells were then harvested and lysed in % Triton X-100 in TBS. The lysates
681 were then added to the Strep affinity gel bound to mmCKAP2 fragments and incubated.
682 The purified proteins were then separated by SDS-PAGE and transferred to nitrocellulose
683 membrane and finally stained with Ponceau and blotted as indicated. The images were

684 adjusted for brightness and contrast for presentation. An experiment representative of two
685 independent biological repeats is shown.
686 F) Alphafold2 model of mmTPX2 (gold) bound to mmCKAP2 (cyan) showing interacting
687 residues labelled in red.
688 **Figure 5: CKAP2 phosphorylation dynamics are required for spindle stability and cell**
689 **proliferation**
690 A) Immunofluorescence images of cells expressing CKAP2 Aurora site mutants fused to
691 mNeon Green. RPE1 CKAP2 KO Clone 8 cells were plated on glass coverslips. They
692 were then transfected with the indicated constructs. The cells were treated with STLC,
693 and after 24 hours of treatment the cells were fixed and stained for β–tubulin. The
694 CKAP2 and β-tubulin channels were adjusted evenly for brightness and contrast. The
695 DAPI channel of each condition was adjusted independently. Representative images from
696 3 independent biological experiments are shown. Scale bars, 10 μm and 1 μm (inset).
697 B) Quantification of the β-tubulin levels from the cells in panel (A). The Z-section with the
698 brightest signal was chosen, and an outline traced around the mitotic spindle. The levels
699 of β-tubulin were then measured. Background signal was taken as the minimum
700 measured value in the mitotic spindle area and subtracted from the measured signal. At
701 least 25 cells per condition for each of 3 independent biological repeats were measured.
702 Error bars indicate the mean +/- SEM. Statistical significance was calculated between the
703 indicated conditions using Dunnett's multiple comparison test.
704 C) Quantification of the spindle diameter of the cells from panel (A). The diameter of the β-
705 tubulin signal was measured for each of the cells quantified in panel (B). Error bars

706 indicate the mean +/- SEM. Statistical significance was calculated between the indicated
707 conditions using Dunnett's multiple comparison test.
708 D) Kymographs of TIRF microscopy images of His-mmCKAP2-GFP-Strep and/or His-
709 mmTPX2-GFP-Strep together with GMPCPP microtubule seeded microtubules.
710 GMPCPP seeds were flowed into a slide chamber and washed. Free tubulin subunits were
711 then flowed into the chamber along with His-mmCKAP2-eGFP-Strep, His-mmTPX2-
712 eGFP-Strep or both proteins together. Images were then taken at the indicated time
713 points. Representative images of one of two independent biological repeats are shown.
714 E) Quantification of the data from (D). The growth rate from at 51 (control) 35 (CKAP2) 32
715 (TPX2) 34 (CKAP2+TPX2) microtubules per condition from two independent
716 experiments were measured and plotted in Prism.
717 F) HeLa cells were plated and then transfected with various mmCKAP2 constructs fused to
718 mNeon Green as indicated. Two days following transfection, 1 μg/ml puromycin was
719 added for 3 days and then changed for 0.2 μg/ml puromycin. 12 days later, the cells were
720 fixed and stained with crystal violet. A single experiment was performed. Scale bar, 4 cm.
721 **Figure 6: Mitotic spindle growth is controlled by an AurKA/TPX2/CKAP2 complex**
722 Cartoon diagram showing how CKAP2 is affected by phosphorylation via an
723 AurKA/TPX2 complex. By itself, CKAP2 robustly mediates microtubule growth and
724 stabilization. During mitosis, CKAP2 is bound by TPX2, which results in
725 phosphorylation via the TPX2 binding partner AurKA. Phosphorylation of CKAP2
726 results in lower microtubule binding affinity and polymerization activity.
727 **Figure S1: AurKB does not co-localize with CKAP2 during mitosis; TPX2 is a CKAP2**
728 **binding partner**

729 A) TPX2 was immunoprecipitated together with interacting proteins from RPE1 cells
730 synchronized via Palbociclib-STLC block. The purified proteins were then separated by
731 SDS-PAGE, transferred to nitrocellulose membrane and blotted as indicated. The panels
732 were adjusted for brightness and contrast. An experiment representative of two
733 independent biological repeats is shown.
734 B) Immunofluorescence images from RPE1 eGFP-CKAP2 cells in various stages of mitosis
735 stained for CKAP2, AurKB, and DAPI. The CKAP2 and AurKB channels were adjusted
736 evenly for brightness and contrast. The DAPI channel of each condition was adjusted
737 independently. Representative images from 2 independent biological experiments are
738 shown. Scale bars, 10 μm and 1 μm (inset).
739 C) Line scans across the indicated paths from the images in panel (B).
740 **Figure S2: PP2A phosphatase activity does not affect CKAP2 mitotic spindle localization**
741 A) Immunofluorescence images from RPE1 cells treated with Okadaic acid. RPE1 cells were
742 plated on glass coverslips and allowed to proliferate. The cells were then treated with
743 DMSO control or 100 nM Okadaic acid for 2 hours before fixation and staining for
744 CKAP2 and β-tubulin. The CKAP2 and β-tubulin channels were adjusted evenly for
745 brightness and contrast. The DAPI channel of each condition was adjusted independently.
746 Representative images from 2 independent biological experiments are shown. Scale bars,
747 10 μm and 1 μm (inset).
748 B) Line scans across the indicated paths from the images in panel (A).
749 C) RPE1 cells were synchronized by Palbociclib-STLC block. The cells were then treated
750 with 100 nM Okadaic acid for 2 hours before harvesting. The cells were then collected
751 and lysed by boiling in SDS-containing buffer. The SDS was then inactivated by 10-fold

752 dilution with 1.5% Triton X-100 buffer. CKAP2 was then purified by
753 immunoprecipitation. The protein G agarose with bound proteins were then boiled in
754 sample buffer to elute purified proteins. Purified proteins were then separated by SDS-
755 PAGE, which was then stained with with ProQ Diamond phosphoprotein stain and
756 imaged. Finally, the gel was stained with Coomassie blue and imaged again. Two
757 independent experiments were performed with similar results.

758 **Figure S3: CKAP2 phosphorylation reduces TPX2/AurKA mitotic spindle localization**

759 A) Immunofluorescence images of cells expressing CKAP2 Aurora site mutants fused
760 to mNeon Green. RPE1 CKAP2 KO Clone 8 cells were plated on glass coverslips.
761 They were then transfected with the indicated constructs. The cells were then treated
762 with STLC, and after 24 hours of treatment the cells were fixed and stained for
763 TPX2. The CKAP2 and TPX2 channels were adjusted evenly for brightness and
764 contrast. The DAPI channel of each condition was adjusted independently.
765 Representative images from 3 independent biological experiments are shown. Scale
766 bars, 10 μm and 1 μm (inset).

767 B) As for panel (A) but the cells were stained for AurKA

768 C) Quantification of the TPX2 levels from the cells in panel (A). The Z-section with the
769 brightest signal was chosen, and an outline traced around the mitotic spindle. The
770 levels of TPX2 were then measured. Background signal was taken as the minimum
771 measured value in the mitotic spindle area and subtracted from the measured signal.
772 At least 25 cells per condition for each of 3 independent biological repeats were
773 measured. Error bars indicate the mean +/- SEM. Statistical significance was

774 calculated between the indicated conditions using Dunnett's multiple comparison
775 test.
776 D) As for panel (C), but the cells from panel (B) were measured and the levels of
777 AurKA quantified.

778 **References**

779 1. Kapoor, T. Metaphase Spindle Assembly. *Biology* **6**, 8 (2017).
780 2. Compton, D. A. SPINDLE ASSEMBLY IN ANIMAL CELLS. (2000).
781 3. Heald, R. & Khodjakov, A. Thirty years of search and capture: The complex simplicity of
782 mitotic spindle assembly. *J. Cell Biol.* **211**, 1103–1111 (2015).
783 4. Bakhoum, S. F. & Compton, D. A. Kinetochores and disease: keeping microtubule dynamics
784 in check! *Curr. Opin. Cell Biol.* **24**, 64–70 (2012).
785 5. Bakhoum, S. F. *et al.* The mitotic origin of chromosomal instability. *Curr. Biol.* **24**, R148–
786 R149 (2014).
787 6. Ertych, N. *et al.* Increased microtubule assembly rates influence chromosomal instability in
788 colorectal cancer cells. *Nat. Cell Biol.* **16**, 779–791 (2014).
789 7. Gomes Paim, L. M. & Bechstedt, S. Regulation of microtubule growth rates and their impact
790 on chromosomal instability. *Cell Cycle* **23**, 872–891 (2024).
791 8. Paim, L. M. G., Lopez-Jauregui, A. A., McAlear, T. S. & Bechstedt, S. The spindle protein
792 CKAP2 regulates microtubule dynamics and ensures faithful chromosome segregation. *Proc.*
793 *Natl. Acad. Sci.* **121**, e2318782121 (2024).
794 9. McAlear, T. S. & Bechstedt, S. The mitotic spindle protein CKAP2 potently increases
795 formation and stability of microtubules. *eLife* **11**, e72202 (2022).
796 10. Yu, G. *et al.* RSK Promotes Prostate Cancer Progression in Bone through ING3, CKAP2,
797 and PTK6-Mediated Cell Survival. *Mol. Cancer Res.* **13**, 348–357 (2015).

798 11. Guo, Q., Song, Y., Hua, K. & Gao, S. Involvement of FAK-ERK2 signaling pathway in
799 CKAP2-induced proliferation and motility in cervical carcinoma cell lines. *Sci. Rep.* **7**, 2117
800 (2017).
801 12. Dos Santos, A., Ouellete, G., Diorio, C., Elowe, S. & Durocher, F. Knockdown of
802 CKAP2 Inhibits Proliferation, Migration, and Aggregate Formation in Aggressive Breast
803 Cancer. *Cancers* **14**, 3759 (2022).
804 13. Hayashi, T. *et al.* Cytoskeleton-associated protein 2 is a potential predictive marker for
805 risk of early and extensive recurrence of hepatocellular carcinoma after operative resection.
806 *Surgery* **155**, 114–123 (2014).
807 14. Yoo, B. H., Kang, D.-S., Park, C.-H., Kang, K. & Bae, C.-D. CKAP2 phosphorylation by
808 CDK1/cyclinB1 is crucial for maintaining centrosome integrity. *Exp. Mol. Med.* **49**, e354–
809 e354 (2017).
810 15. Seki, A. & Fang, G. CKAP2 Is a Spindle-associated Protein Degraded by APC/C-Cdh1
811 during Mitotic Exit. *J. Biol. Chem.* **282**, 15103–15113 (2007).
812 16. Hong, K. U. *et al.* Cdk1-Cyclin B1-mediated Phosphorylation of Tumor-associated
813 Microtubule-associated Protein/Cytoskeleton-associated Protein 2 in Mitosis. *J. Biol. Chem.*
814 **284**, 16501–16512 (2009).
815 17. Hong, K. U., Kim, H.-J., Bae, C.-D. & Park, J. Characterization of mitosis-specific
816 phosphorylation of tumor-associated microtubule-associated protein. *Exp. Mol. Med.* **41**, 832
817 (2009).
818 18. Hong, K. U. *et al.* Transient phosphorylation of tumor associated microtubule associated
819 protein (TMAP)/cytoskeleton associated protein 2 (CKAP2) at Thr-596 during early phases of
820 mitosis. *Exp. Mol. Med.* **40**, 377 (2008).

821 19. Kim, H.-J., Kwon, H.-R., Bae, C.-D., Park, J. & Hong, K. U. Specific primary sequence
822 requirements for Aurora B kinase-mediated phosphorylation and subcellular localization of
823 TMAP during mitosis. *Cell Cycle* **9**, 2027–2036 (2010).
824 20. Hong, K. U. *et al.* Functional Importance of the Anaphase-Promoting Complex-Cdh1-
825 Mediated Degradation of TMAP/CKAP2 in Regulation of Spindle Function and Cytokinesis.
826 *Mol. Cell. Biol.* **27**, 3667–3681 (2007).
827 21. Kettenbach, A. N. *et al.* Quantitative Phosphoproteomics Identifies Substrates and
828 Functional Modules of Aurora and Polo-Like Kinase Activities in Mitotic Cells. *Sci. Signal.* **4**,
829 rs5–rs5 (2011).
830 22. Olsen, J. V. *et al.* Quantitative Phosphoproteomics Reveals Widespread Full
831 Phosphorylation Site Occupancy During Mitosis. *Sci. Signal.* **3**, ra3–ra3 (2010).
832 23. Kucharski, T. J. *et al.* An Aurora kinase A-BOD1L1-PP2A B56 axis promotes
833 chromosome segregation fidelity. *Cell Rep.* **44**, 115317 (2025).
834 24. Karthigeyan, D., Prasad, S. B. B., Shandilya, J., Agrawal, S. & Kundu, T. K. Biology of
835 Aurora A kinase: Implications in cancer manifestation and therapy: BIOLOGY OF AURORA
836 A KINASE. *Med. Res. Rev.* **31**, 757–793 (2011).
837 25. Barr, A. R. & Gergely, F. Aurora-A: the maker and breaker of spindle poles. *J. Cell Sci.*
838 **120**, 2987–2996 (2007).
839 26. Nikonova, A. S., Astsaturov, I., Serebriiskii, I. G., Dunbrack, R. L. & Golemis, E. A.
840 Aurora A kinase (AURKA) in normal and pathological cell division. *Cell. Mol. Life Sci.* **70**,
841 661–687 (2013).

842 27. Carmena, M., Ruchaud, S. & Earnshaw, W. C. Making the Auroras glow: regulation of
843 Aurora A and B kinase function by interacting proteins. *Curr. Opin. Cell Biol.* **21**, 796–805
844 (2009).
845 28. Kufer, T. A. *et al.* Human TPX2 is required for targeting Aurora-A kinase to the spindle.
846 *J. Cell Biol.* **158**, 617–623 (2002).
847 29. Zhang, R., Roostalu, J., Surrey, T. & Nogales, E. Structural insight into TPX2-stimulated
848 microtubule assembly. *eLife* **6**, e30959 (2017).
849 30. Brunet, S. *et al.* Characterization of the TPX2 Domains Involved in Microtubule
850 Nucleation and Spindle Assembly in *Xenopus* Egg Extracts. *Mol. Biol. Cell* **15**, 5318–5328
851 (2004).
852 31. Bischoff, J. R. A homologue of Drosophila aurora kinase is oncogenic and amplified in
853 human colorectal cancers. *EMBO J.* **17**, 3052–3065 (1998).
854 32. Zhou, H. *et al.* Tumour amplified kinase STK15/BTAK induces centrosome
855 amplification, aneuploidy and transformation. *Nat. Genet.* **20**, 189–193 (1998).
856 33. Sen, S., Zhou, H. & White, R. A. A putative serine/threonine kinase encoding gene
857 BTAK on chromosome 20q13 is ampli®ed and overexpressed in human breast cancer cell
858 lines.
859 34. Reid, T. A. *et al.* Suppression of microtubule assembly kinetics by the mitotic protein
860 TPX2. *J. Cell Sci.* jcs.178806 (2016) doi:10.1242/jcs.178806.
861 35. Wheelock, M. S., Wynne, D. J., Tseng, B. S. & Funabiki, H. Dual recognition of
862 chromatin and microtubules by INCENP is important for mitotic progression. *J. Cell Biol.*
863 **216**, 925–941 (2017).

864 36. Broad, A. J., DeLuca, K. F. & DeLuca, J. G. Aurora B kinase is recruited to multiple
865 discrete kinetochore and centromere regions in human cells. *J. Cell Biol.* **219**, e201905144
866 (2020).
867 37. Krenn, V. & Musacchio, A. The Aurora B Kinase in Chromosome Bi-Orientation and
868 Spindle Checkpoint Signaling. *Front. Oncol.* **5**, (2015).
869 38. Eyers, P. A., Erikson, E., Chen, L. G. & Maller, J. L. A Novel Mechanism for Activation
870 of the Protein Kinase Aurora A. *Curr. Biol.* **13**, 691–697 (2003).
871 39. Bayliss, R., Sardon, T., Vernos, I. & Conti, E. Structural Basis of Aurora-A Activation by
872 TPX2 at the Mitotic Spindle. *Mol. Cell* **12**, 851–862 (2003).
873 40. A. B. Dounay & C. J. Forsyth. Okadaic Acid: The Archetypal Serine / Threonine Protein
874 Phosphatase Inhibitor. *Curr. Med. Chem.* **9**, 1939–1980 (2002).
875 41. Takai, A. *et al.* Inhibitory effect of okadaic acid derivatives on protein phosphatases. A
876 study on structure-affinity relationship. *Biochem. J.* **284**, 539–544 (1992).
877 42. Kucharski, T. J. Chromosome segregation fidelity is controlled by small changes in
878 phospho-occupancy at the kinetochore-microtubule interface. *J. Cell Biol.* (2022).
879 43. Zaytsev, A. V. *et al.* Multisite phosphorylation of the NDC80 complex gradually tunes its
880 microtubule-binding affinity. *Mol. Biol. Cell* **26**, 1829–1844 (2015).
881 44. DeLuca, K. F., Lens, S. M. A. & DeLuca, J. G. Temporal changes in Hec1
882 phosphorylation control kinetochore-microtubule attachment stability during mitosis. *J. Cell*
883 *Sci.* **124**, 622–634 (2011).
884 45. Guimaraes, G. J., Dong, Y., McEwen, B. F. & DeLuca, J. G. Kinetochore-Microtubule
885 Attachment Relies on the Disordered N-Terminal Tail Domain of Hec1. *Curr. Biol.* **18**, 1778–
886 1784 (2008).

887 46. Lyalina, T., Paim, L. M. G. & Bechstedt, S. Enzymatic Function of an Intrinsically
888 Disordered Protein.
889 47. Yang, Z., Zeng, X., Zhao, Y. & Chen, R. AlphaFold2 and its applications in the fields of
890 biology and medicine. *Signal Transduct. Target. Ther.* **8**, 115 (2023).
891 48. Hengeveld, R. C. C. *et al.* Development of a Chemical Genetic Approach for Human
892 Aurora B Kinase Identifies Novel Substrates of the Chromosomal Passenger Complex. *Mol.*
893 *Cell. Proteomics* **11**, 47–59 (2012).
894 49. Perez-Riverol, Y. *et al.* The PRIDE database resources in 2022: a hub for mass
895 spectrometry-based proteomics evidence. *Nucleic Acids Res.* **50**, D543–D552 (2022).
896 50. Geu-Flores, F., Nour-Eldin, H. H., Nielsen, M. T. & Halkier, B. A. USER fusion: a rapid
897 and efficient method for simultaneous fusion and cloning of multiple PCR products. *Nucleic*
898 *Acids Res.* **35**, e55–e55 (2007).
899 51. Kucharski, T. J., Minshall, P. E., Moustafa-Kamal, M., Turnell, A. S. & Teodoro, J. G.
900 Reciprocal Regulation between 53BP1 and the Anaphase-Promoting Complex/Cyclosome Is
901 Required for Genomic Stability during Mitotic Stress. *Cell Rep.* **18**, 1982–1995 (2017).
902 52. Ashford, A. J., Andersen, S. L. A. & Hyman, A. A. Preparation of Tubulin from Bovine
903 Brain. in *Cell Biology, a Laboratory Handbook* vol. 2 205–212 (Academic Press, New York,
904 1998).
905 53. Hyman, A. *et al.* Preparation of Modified Tubulins. *METHODS Enzymol.* **196**, 478–485
906 (1991).
907 54. Schindelin, J. *et al.* Fiji: an open-source platform for biological-image analysis. *Nat.*
908 *Methods* **9**, 676–682 (2012).
909

Kucharski *et al.* Figure 1

A

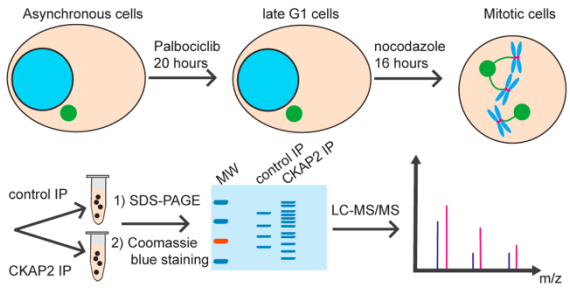

B

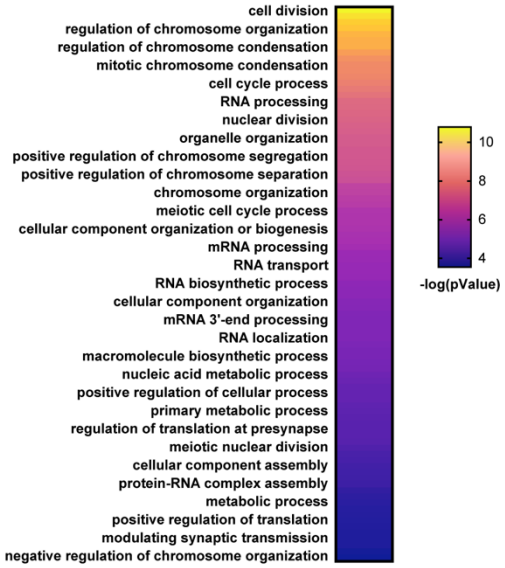

C

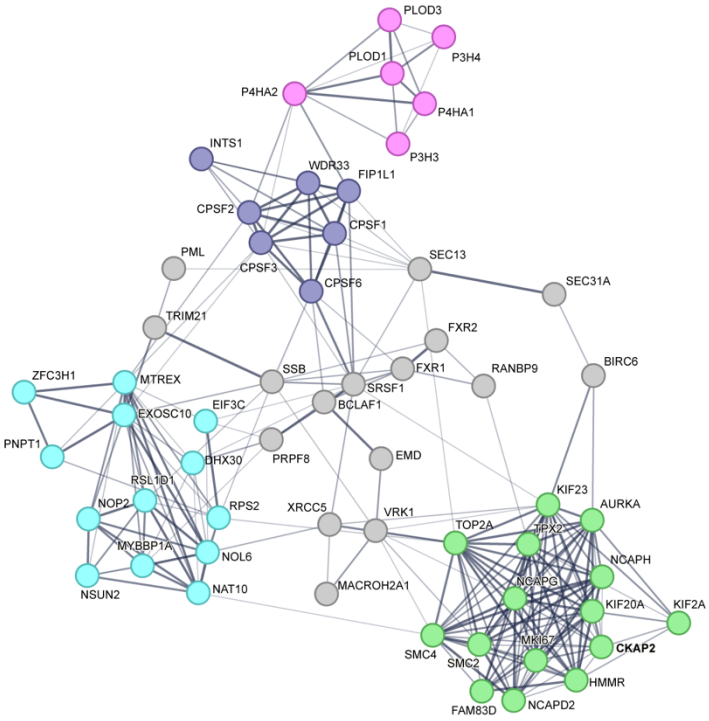

D

Protein ID	Number of peptides in CKAP2 IP	Number of peptides in control IP
CKAP2	68	0
SEC31A	63	0
MTREX	43	1
ZFC3H1	42	0
TOP2A	41	0
KIF2A	28	0
TXLNA	27	0
CPSF1	25	0
CPSF2	22	0
DOCK7	21	0
BIRC6	19	0
SMC2	18	0
SMC4	17	0
NCAPG	10	0
MACROH2A1	9	0
KIF20A	8	1
TPX2	7	0
NCAPD2	6	0
AURKA	4	1

E

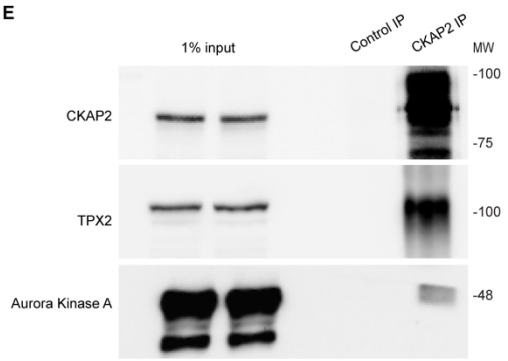

910

Kucharski *et al.* Figure 2

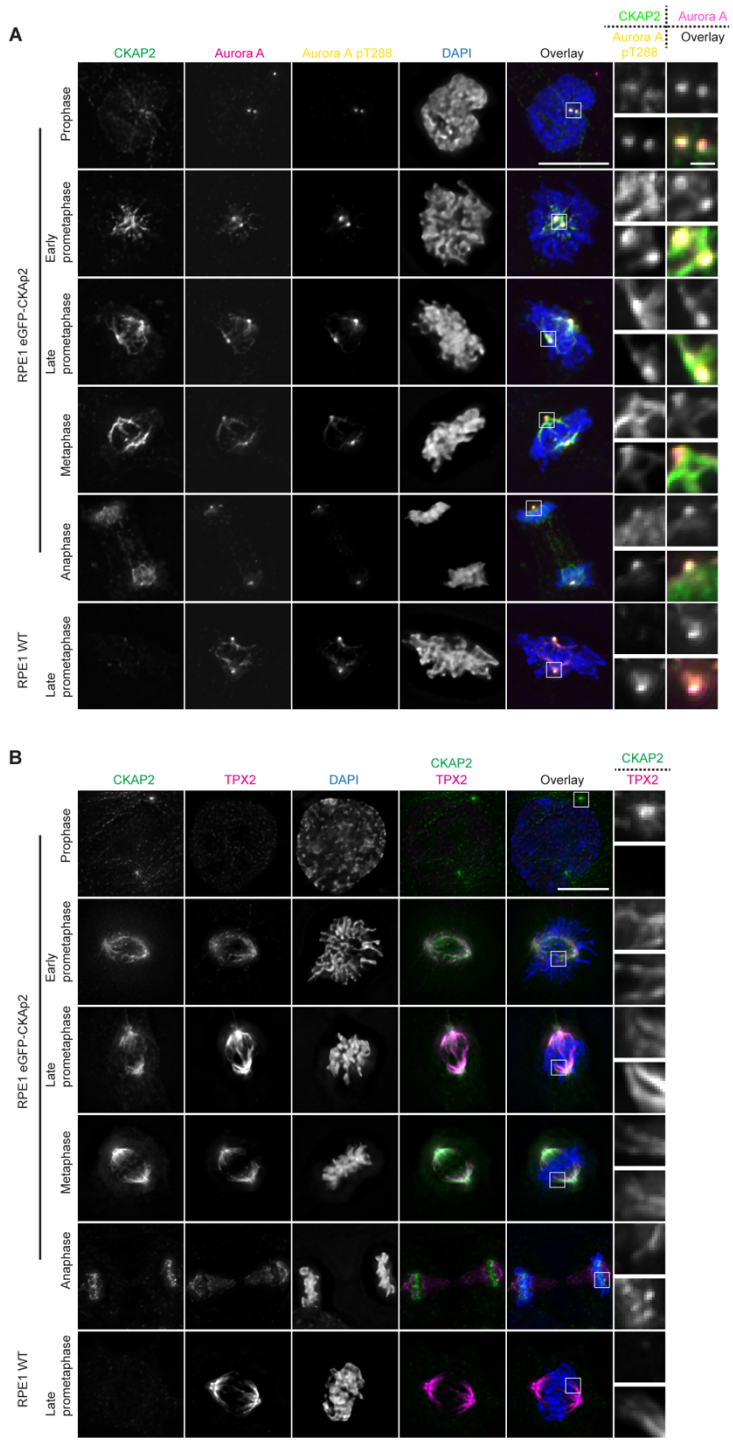

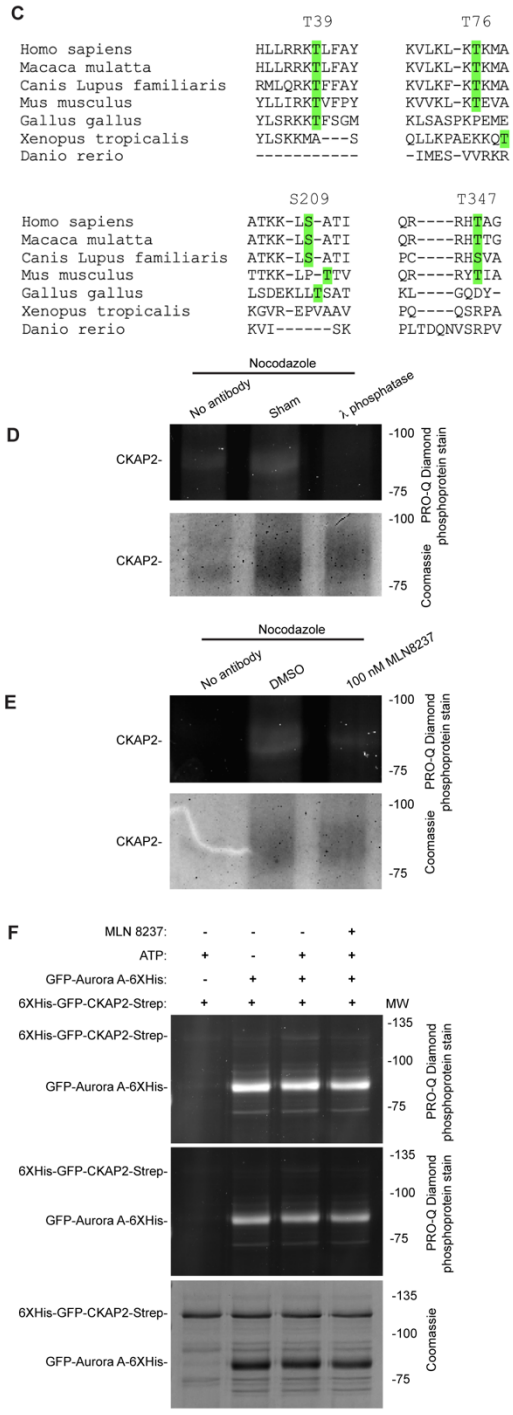

911

Kucharski *et al.* Figure 3

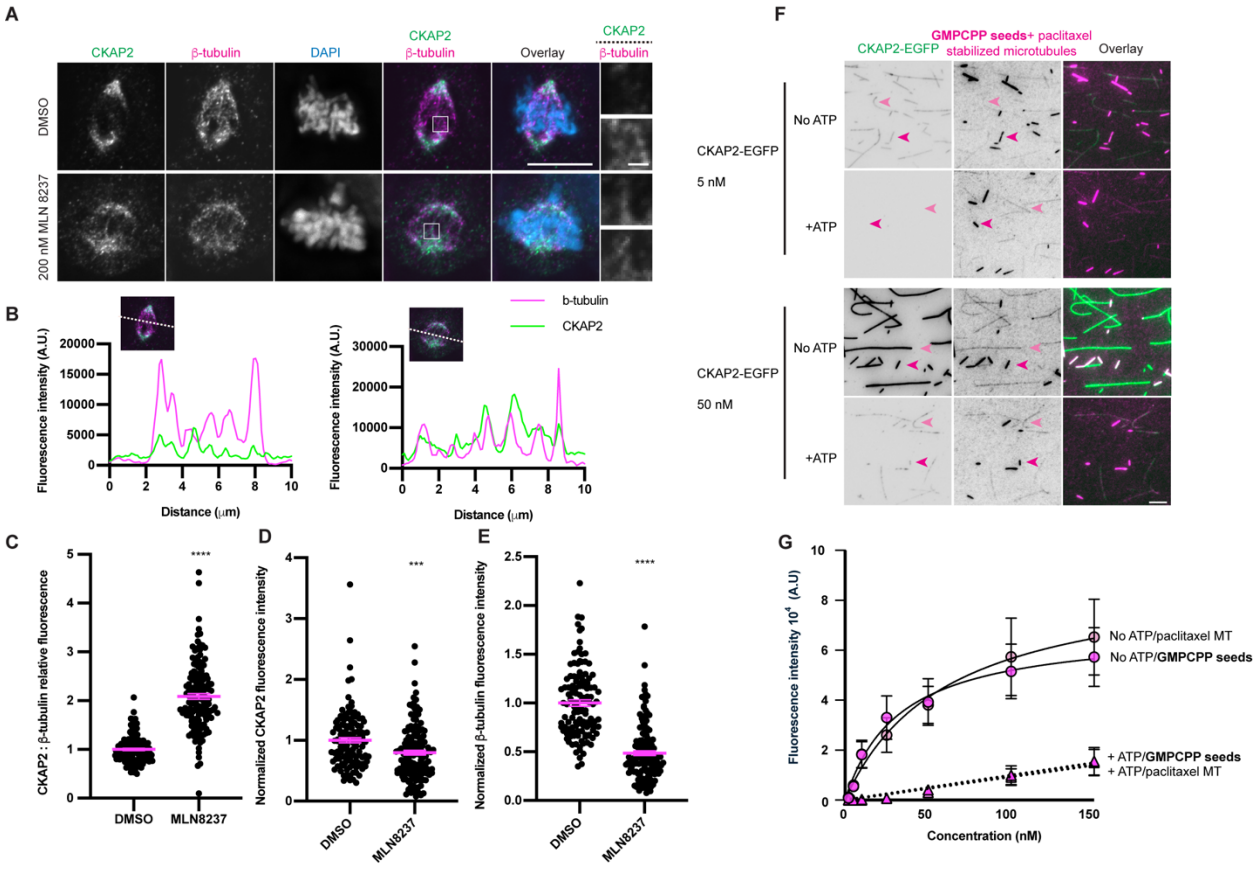

912

Kucharski *et al.* Figure 4

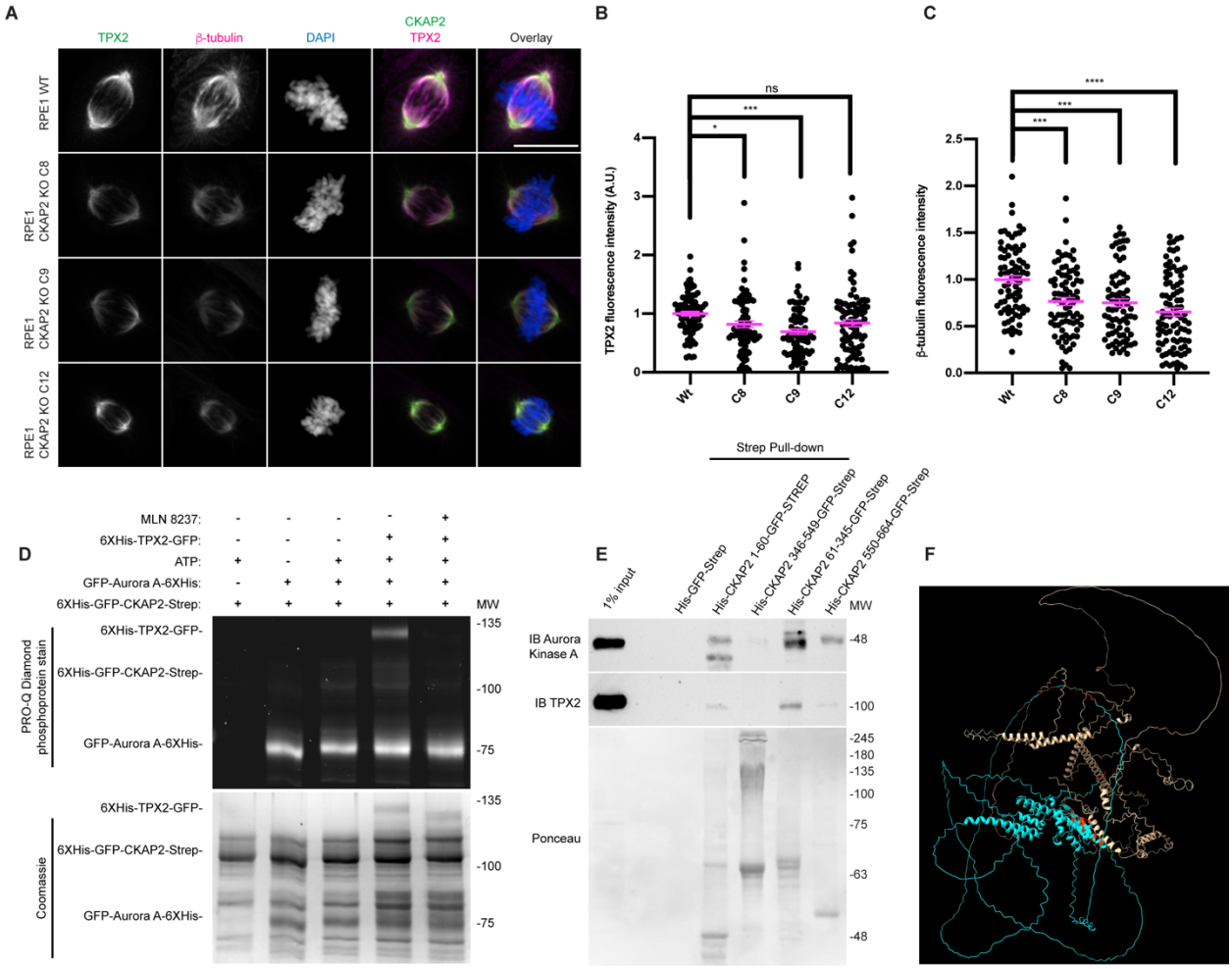

913

Kucharski *et al.* Figure 5

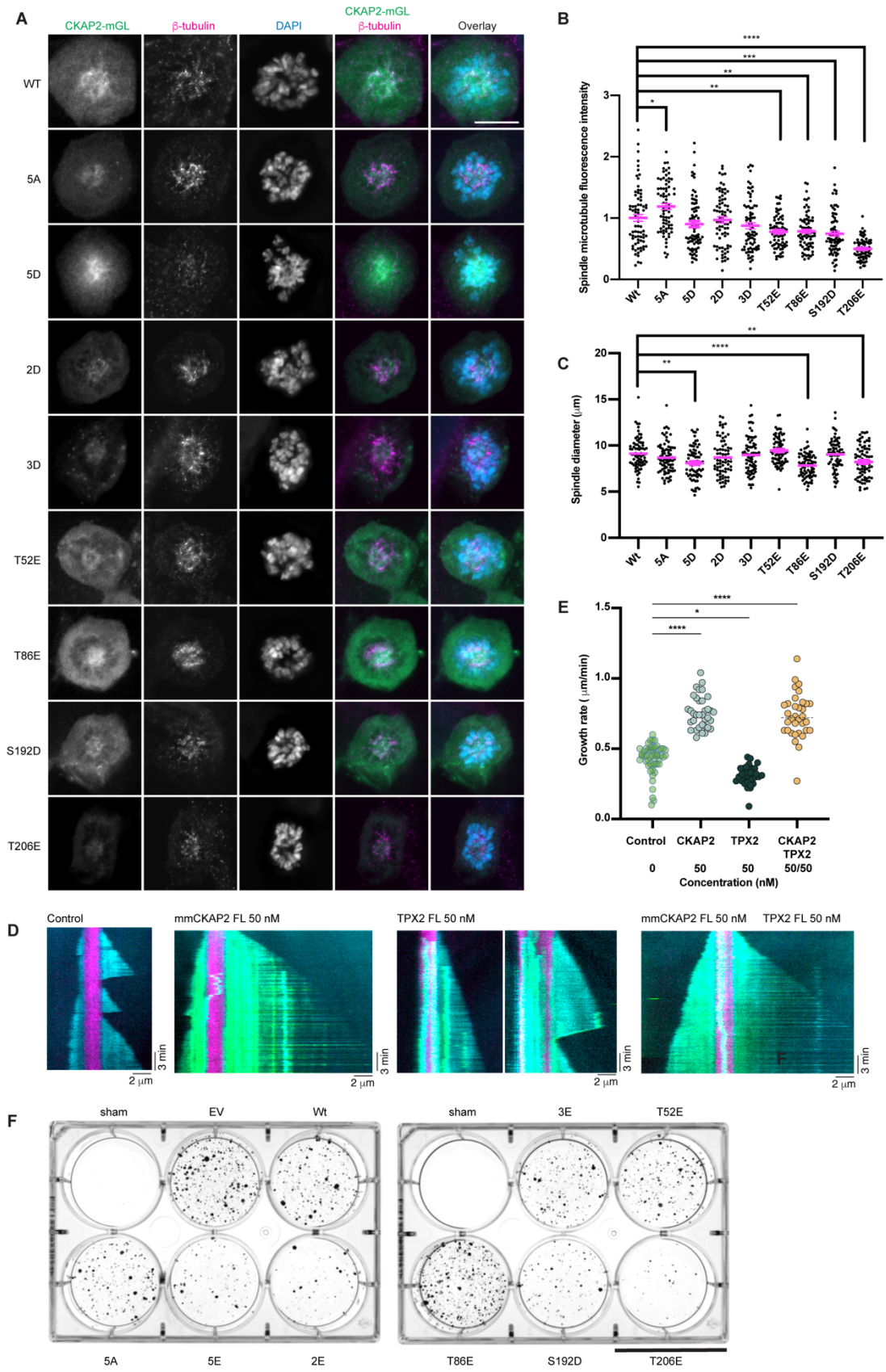

914

Kucharski *et al.* Figure 6

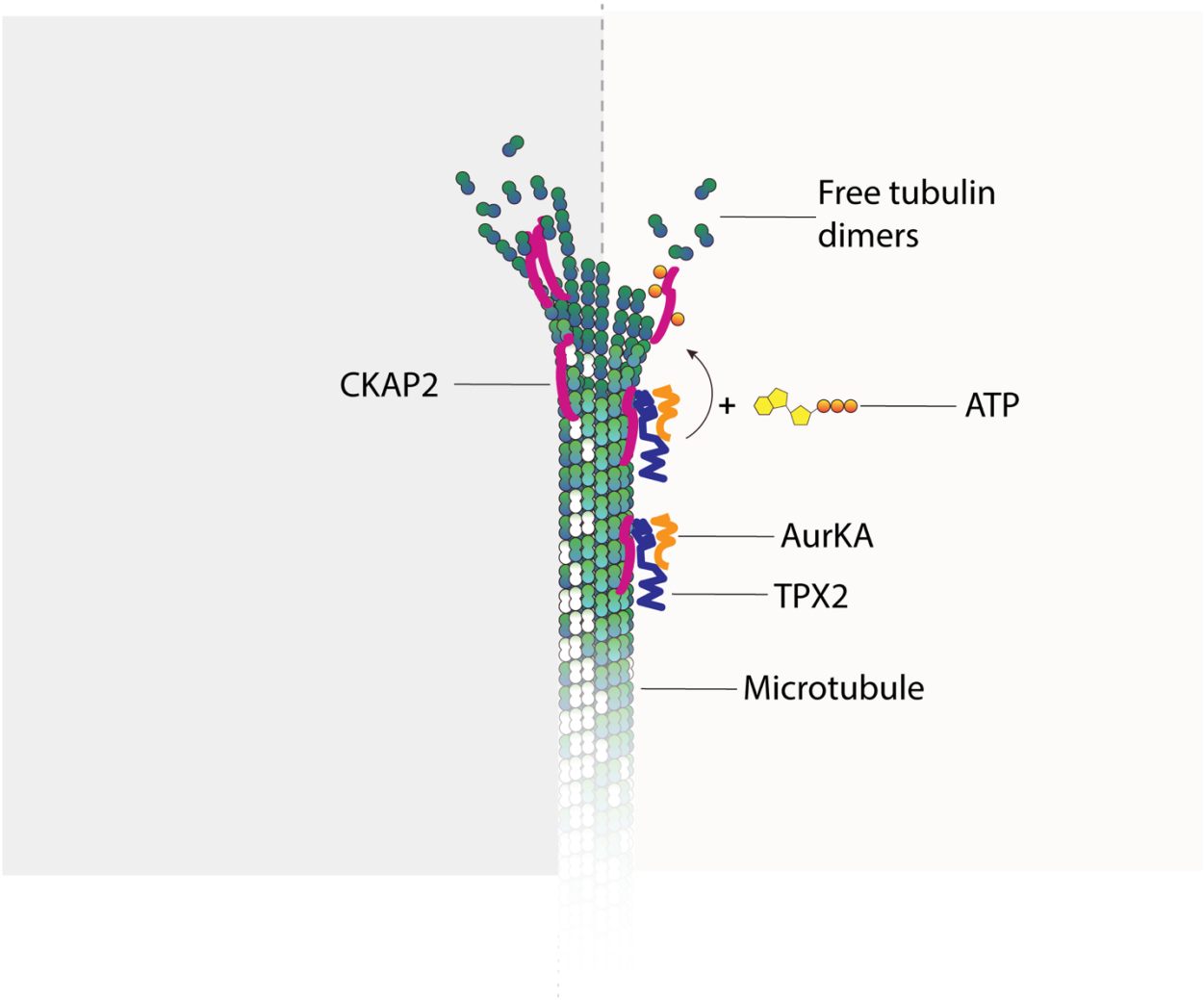

915

Kucharski *et al.* Figure S1

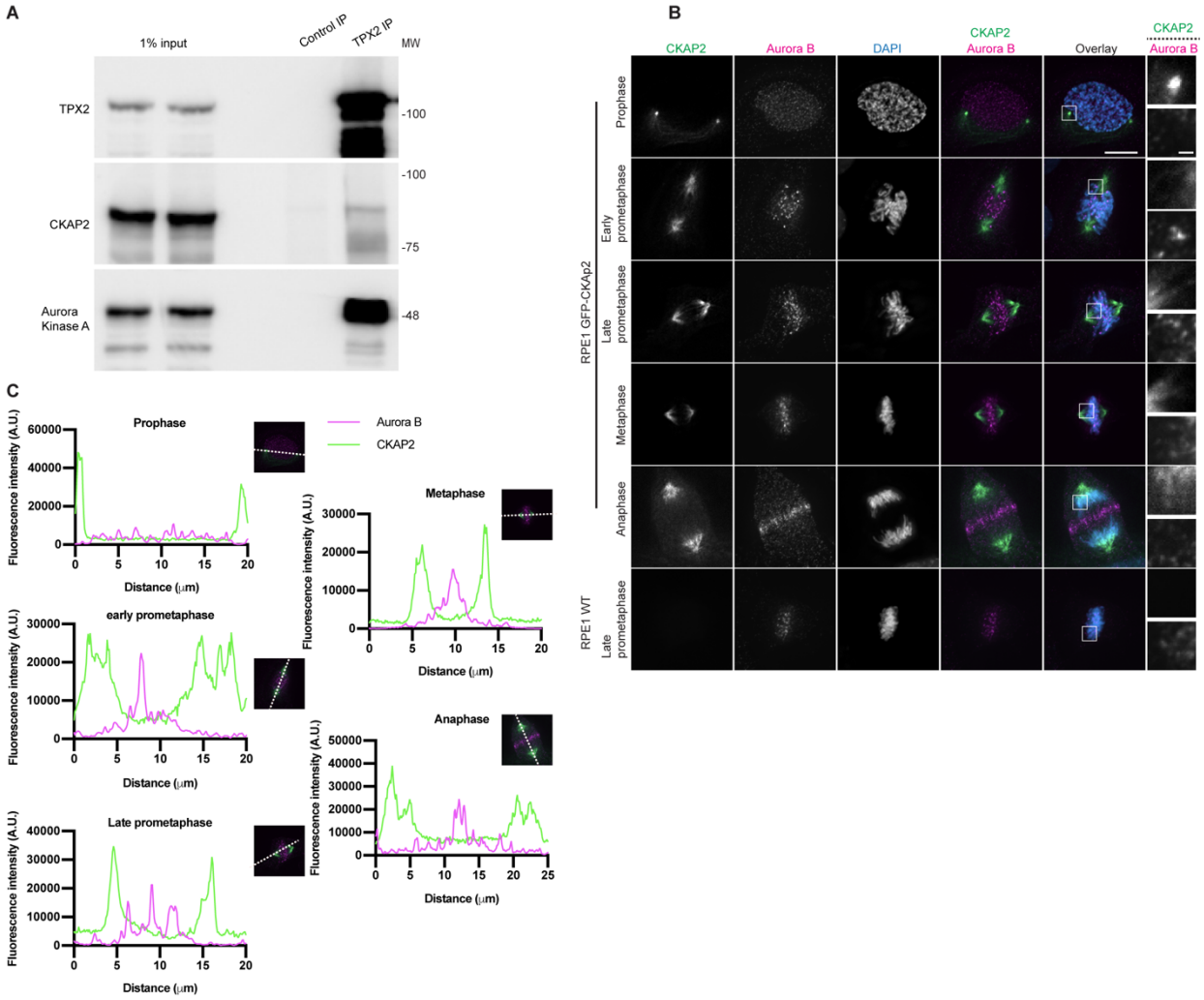

916

Kucharski *et al.* Figure S2

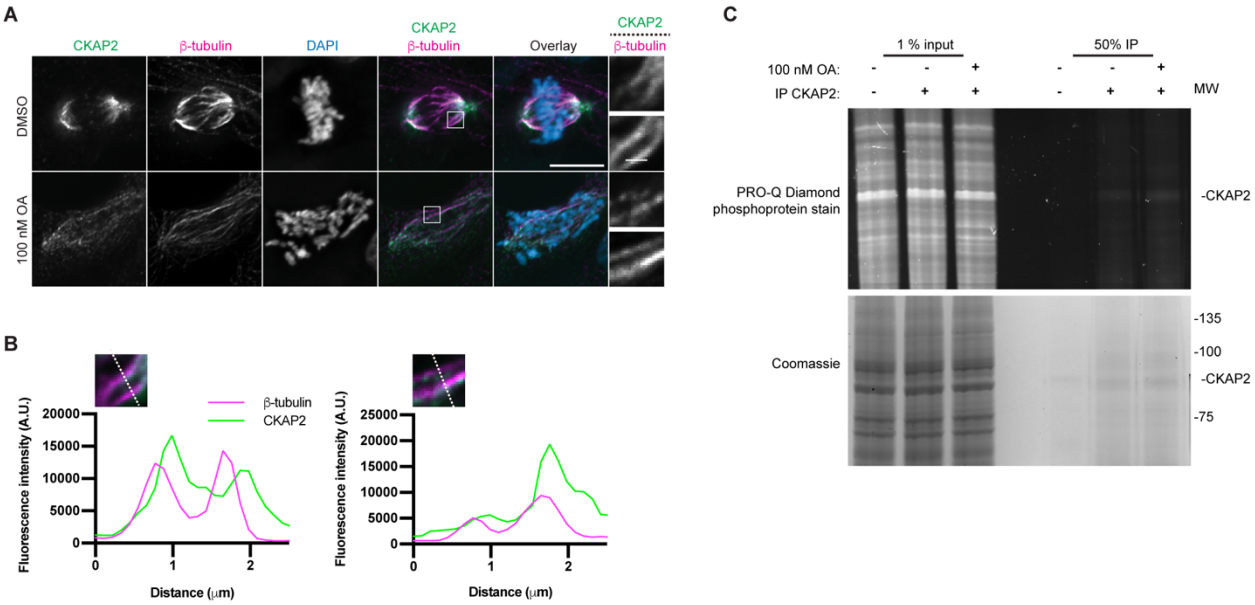

917
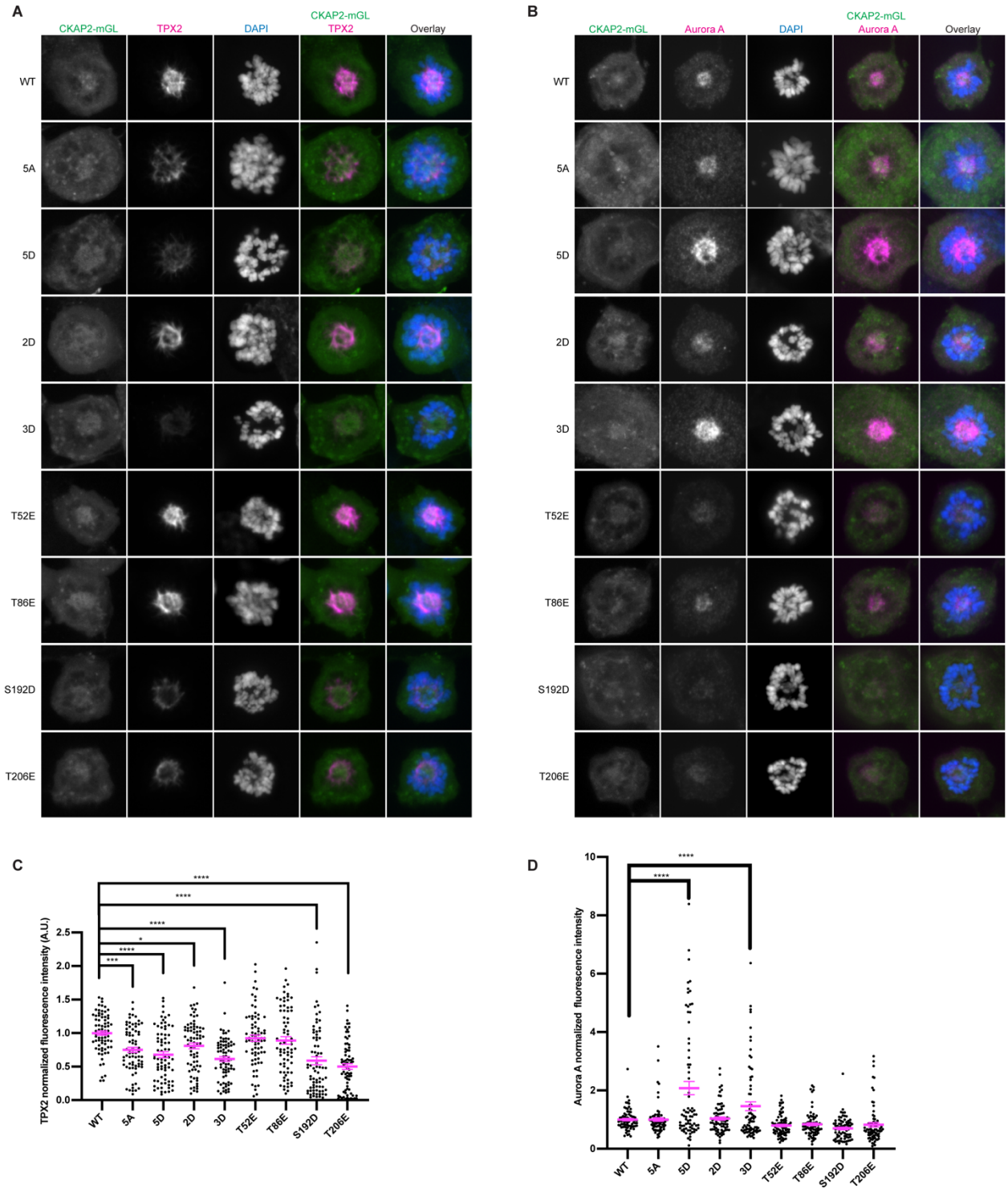
Kucharski *et al*. Figure S3